

1 a Coriolis tutorial, Part 3:
2 β -effects; westward propagation

3 James F. Price

4 Woods Hole Oceanographic Institution,
5 Woods Hole, Massachusetts, 02543

6 www.whoi.edu/science/PO/people/jprice jprice@whoi.edu

7 Version 5

October 15, 2018

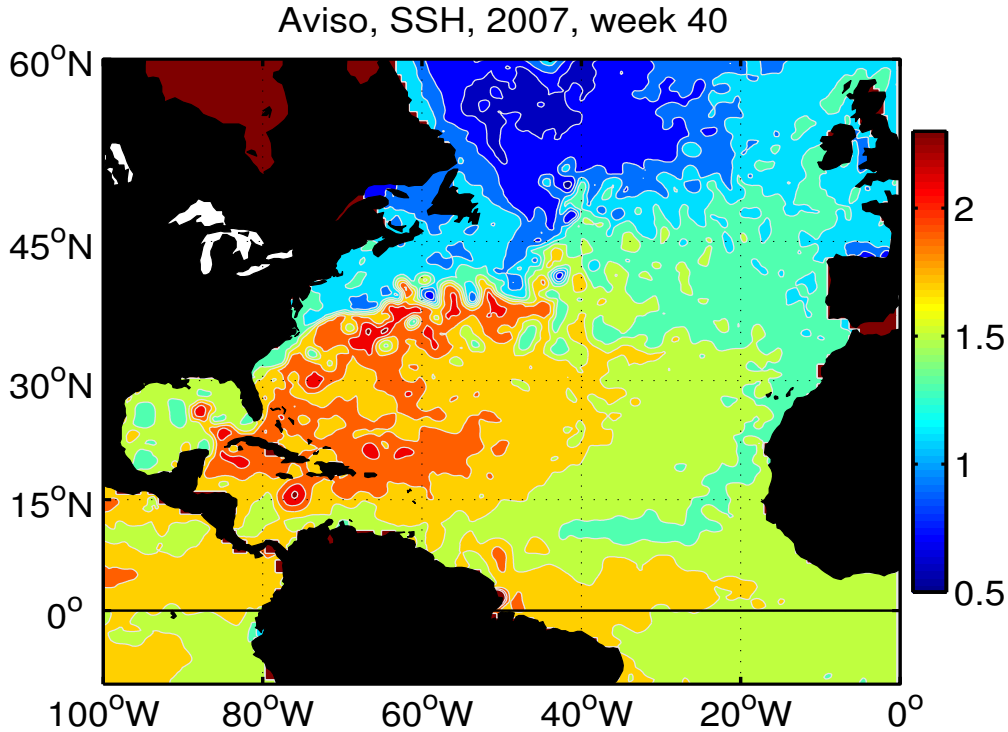


Figure 1: Sea surface height (SSH) over the North Atlantic averaged over one week. The color scale at right is in meters. To animate: www.whoi.edu/jpweb/Aviso-NA2007.flv The largest SSH variability occurs primarily on two spatial scales — basin scale gyres (thousands of kilometers), a high in the subtropics and a low in the subpolar basin — and mesoscale eddies (several hundred kilometers) that are both highs and lows. The basin scale gyres are clearly present on time average, while mesoscale eddies are significantly time-dependent, including marked westward propagation. An understanding of β -effects will greatly enhance your appreciation of these remarkable observations.

8 **Abstract:** This is the third of a four-part introduction to the effects of Earth's rotation on the fluid
9 dynamics of the atmosphere and ocean. The goal is to understand some of the very important beta effects
10 (β -effects) that follow from the northward increase of the Coriolis parameter, f , in linear approximation,
11 $f = f_o + \beta y$. The first problem considered is mid-latitude geostrophic adjustment configured as in Part 2.
12 The short term (less than one week) results are much the same as found on an f -plane, *viz.*, spreading
13 inertia-gravity waves that leave behind a nearly geostrophically balanced eddy. On an f -plane, such an
14 eddy could be exactly steady (absent diffusion or friction). On a β -plane, the same eddy will
15 spontaneously translate westward at a slow and almost steady rate, about 3 km per day at 30° latitude
16 (south or north) and given scales that are typical of oceanic mesoscale eddies. This westward eddy
17 translation has a great deal in common with the propagation of an elementary, long Rossby wave. It is
18 also consistent with the observed propagation of oceanic mesoscale eddies.

19 A similar adjustment experiment set in an equatorial region gives quite different results. Even fairly
20 large, unbalanced thickness anomalies are rapidly dispersed into east and west-going waves. The
21 west-going waves include the equivalent of inertia-gravity and Rossby waves. Long equatorial Rossby
22 waves are nondispersive and have a phase and group speed of about 100 km per day, or 30 times the
23 mid-latitude Rossby wave speed. The east-going Kelvin wave is still more impressive, as it carries the
24 majority of the thickness anomaly in a single, nondispersive pulse that propagates eastward at the gravity
25 wave speed, 300 km per day. Hence, Kelvin waves may transmit signals from mid-ocean to the eastern
26 boundary within about a month.

27 These and other low frequency phenomenon are often interpreted most fruitfully as an aspect of
28 potential vorticity conservation, the geophysical fluid equivalent of angular momentum conservation.
29 Earth's rotation contributes planetary vorticity, f , that is generally considerably larger than the relative
30 vorticity of winds and currents. Small changes in the latitude of a fluid column may convert planetary
31 vorticity to a significant change of relative vorticity, or, if the horizontal scale of the motion is large
32 compared to the radius of deformation, to a change in layer thickness (vortex stretching). The latter is the
33 principal mechanism of westward propagation of long Rossby waves and of the mesoscale eddies studied
34 here.

35 **More on Figure 1:** A one week average of SSH observed by satellite over the North Atlantic ocean
36 (data are thanks to the Aviso project). This SSH is with respect to a level surface, and tides and high
37 frequency variability have been removed. A slowly-varying, tilted SSH implies a geostrophic current that
38 is approximately parallel to isolines of SSH. Along with geostrophic currents there may also be
39 wind-driven Ekman currents that are not directly visible in this field. Compared with the year-long mean
40 of Fig. 1, Part 1, this field shows considerable variability on scales of several hundred kilometers, often
41 termed the oceanic mesoscale.

42 **Contents**

43 **1 Large-scale flows of the atmosphere and ocean; a second look** **4**

44 1.1 Anisotropic, low frequency phenomena 4

45 1.2 Goals and plan of this essay 5

46 **2 Adjustment and propagation on a mid-latitude β -plane** **6**

47 2.1 What’s up with this β -plane? 7

48 2.2 Potential vorticity conservation 10

49 2.3 Planetary Rossby waves 14

50 2.3.1 Beta and relative vorticity; short Rossby waves 18

51 2.3.2 Beta and vortex stretching; long Rossby waves 19

52 2.4 Finite amplitude effects, and the dual identity of mesoscale eddies 21

53 2.4.1 Eddy propagation seen in the η and \mathbf{V} fields 21

54 2.4.2 Fluid transport seen in tracer fields and float trajectories 24

55 2.5 Rossby waves \rightarrow Eddies 28

56 2.6 Some of the varieties of Rossby wave-like phenomenon 31

57 2.6.1 Westerly waves 31

58 2.6.2 Basin-scale Rossby waves 31

59 2.6.3 Topographic eddies and waves 32

60 2.6.4 Tropical cyclones 34

61 2.7 Problems 35

62 **3 Adjustment on an equatorial β -plane** **36**

63 3.1 An equatorial adjustment experiment 36

64 3.2 An equatorial radius of deformation 37

65 3.3 Dispersion relation of equatorially-trapped waves 39

66 3.3.1 Westward-going gravity and Rossby waves 42

67 3.3.2 Kelvin wave 42

68 3.4 Problems 46

69 **4 Summary and Remarks** **46**

70 4.1 Mid-latitude mesoscale eddies 46

71 4.2 Equatorial Adjustment 47

72 4.3 Remarks 48

73 4.4 What's next? 49
74 Index 49

75 1 Large-scale flows of the atmosphere and ocean; a second look

76 This essay is the third of a four part introduction to fluid dynamics on a rotating Earth. Part 1 examined
77 the origin and fundamental properties of the Coriolis force, and went on to consider a few of its
78 consequences for the motion of a single parcel, viz., inertial and geostrophic motion. Part 2 introduced
79 the shallow water model, and examined the circumstances that lead to a near geostrophic balance, a
80 defining characteristic of large scale, low frequency (extra-equatorial) geophysical flow.

81 1.1 Anisotropic, low frequency phenomena

82 A thorough-going understanding (intuition) of the Coriolis force and geostrophy are a good starting point
83 for a study of the atmosphere and ocean. However, geostrophy is nowhere near the end of the road: an
84 exact geostrophic balance (geostrophy on an f-plane, as in Part 2) implies exactly steady winds and
85 currents. Moreover, f-plane phenomena are intrinsically isotropic, showing no favored direction. In
86 sharp contrast to these f-plane properties, observations from the atmosphere and the ocean show that
87 nearly geostrophic winds and currents evolve slowly but continually, even absent external forcing, and
88 they often exhibit a marked anisotropy of one or more properties. Three important examples evident in
89 Fig. 1 and studied here and in the following essay include:

90 Mesoscale Eddies (Sec. 2) Most subtropical and subpolar ocean basins are full of slowly revolving
91 eddies having a radius of O(100 km) and time scales (periods) of several months. Unlike the gyres,
92 eddies do not show a marked asymmetry in their plan view. However, over the open ocean, mesoscale
93 eddies exhibit a slow but steady westward propagation at a rate that varies systematically with latitude; at
94 30°N, about 3 km per day (see the animation linked in the caption of Fig. 1).

95 Equatorial variability (Sec. 3) The SSH variability seen in the equatorial region (±15° of the
96 equator) is quite different from that seen at higher latitudes. Mesoscale eddies are, by comparison with
97 higher latitudes, uncommon. SSH variability occurs primarily in zonally elongated and meridionally
98 compressed features that are displaced from the equator by 5 to 10° and that appear to have significant

99 seasonality. There are occasional events of rapid eastward propagation along the equator, several hundred
100 kilometers per day, sometimes spanning almost the entire basin.

101 **Ocean Gyres** Fig. 1 is centered on the subtropical gyre, a high pressure (high SSH) clockwise rotating,
102 basin-filling circulation that is driven by the overlying winds. A striking characteristic of all wind-driven
103 ocean gyres is that they are strongly compressed onto the western side of the basin, often termed western
104 intensification. This and other aspects of wind-driven circulation will be deferred to Part 4.

105 1.2 Goals and plan of this essay

106 The goal of this essay is to take the next big step beyond geostrophy and address

107 **What process(es) lead to the time-dependence and marked east-west asymmetry of**
108 **most large-scale flow phenomena?**

109 There are many processes that can cause departures from geostrophy and time-dependence, including
110 drag on an upper or lower boundary, which will be considered here in a simplified form. However,
111 another process(es), called the β -effect, is the primary topic. β -effects are ubiquitous in that they arise
112 merely from north-south flow in combination with the northward increase of the Coriolis parameter,

$$113 \quad f(\phi) = 2\Omega \sin \phi, \quad (1)$$

114 where ϕ is the latitude.

115 The $f(\phi)$ above could be used as is in the numerical model, but for a number of reasons it is helpful
116 to utilize the linear approximation that

$$117 \quad f(y) = f(\phi_o) + \frac{df}{dy}y + HOT, \quad (2)$$

118 where $y = R_E(\phi - \phi_o)$ is the north-south (Cartesian) coordinate, R_E is Earth's nominal radius, approx.
119 6370 km, the coefficient of the linear term is almost always called 'beta', and

$$120 \quad \boxed{\beta = \frac{df}{dy} = \frac{2\Omega}{R_E} \cos \phi_o} \quad (3)$$

121 When the higher order terms (HOT) of (2) are ignored, the resulting linear model

$$122 \quad \boxed{f(y) = f(\phi_o) + \beta y} \quad (4)$$

123 is often called a β -plane. β is positive in both hemispheres, has a maximum at the equator, and goes to
124 zero at the poles. At 30° N, say, $\beta = 2.29 \times 10^{-11} \text{ m}^{-1} \text{ s}^{-1}$, which looks to be very small. However, the
125 appropriate comparison is βy with the constant term $f_o = f(\phi_o)$ of (2), and then it is apparent that the β
126 term is $\propto \delta y / R_E$, where δy is the north-south scale of the phenomenon under analysis. The β term is still
127 small for mesoscale-sized phenomena, $\delta y = O(10^5)$ m, however, β effects may be systematic and
128 persistent and thus may become very important over a long term, months.

129 The plan is to solve and analyze a sequence of idealized numerical experiments posed in a shallow
130 water (single layer fluid) model in which the Coriolis parameter is represented by the β -plane
131 approximation, Eqn. (4). The shallow water momentum and continuity equations were written in Sec. 2,
132 Part 2 and will not be repeated until some new terms are added in Part 4. The configuration used in Secs.
133 2 and 3 are adjustment experiments in an open domain, very much like those of Part 2. Mid-latitude,
134 mesoscale eddies are treated in Sec. 2. A similar equatorial adjustment experiment is considered in Sec.
135 3.

136 The emphasis here is on β -effects rather than the shallow water model *per se*. There are, however,
137 two aspects of the model and method that you should watch for (noted also in Part 2). First, the shallow
138 water equations solved here are nonlinear, in common with all but the most simplified fluid models.
139 Whether that results in appreciable finite amplitude phenomena depends in part upon the amplitude of the
140 initial eddy (Sec. 2) or wind stress (Part 4). Here these amplitudes were chosen to be realistic of the
141 phenomena of Fig. 1, and as a result, finite amplitude effects are appreciable but generally not dominant.
142 However, this assessment depends very much on the specific phenomenon under consideration, i.e.,
143 whether eddy propagation, which looks to be nearly linear, or parcel displacement, which is significantly
144 nonlinear. In the best of cases, an interpretation can start from a linear perspective and then treat finite
145 amplitude effects as perturbations. Second, the primary analysis method is diagnosis of the potential
146 vorticity balance, i.e. q -balance. This was very fruitful for understanding the geostrophic adjustment
147 phenomena of Part 2, and it is almost indispensable for interpretation of the upcoming experiments.
148 Having some fluency with q -balance will be invaluable for your study of oceanic and atmospheric
149 dynamics, and an important, implicit goal of this essay is to help you make a start.

150 **2 Adjustment and propagation on a mid-latitude β -plane**

151 The SSH data of Fig. 1 (and especially its animation linked in the caption) reveal a number of important
152 properties of the mesoscale eddy field:

153 **1) Eddy scales.** Any given snapshot of SSH will show widespread variability in the form of more or less

154 circular SSH anomalies having a radius $L \approx 100$ km and an amplitude of typically ± 0.1 m and currents
 155 $U \approx 0.1$ m sec⁻¹ — mesoscale eddies. A given eddy, i.e., a specific SSH anomaly, can often be identified
 156 and tracked for many months. Direct measurements of ocean currents within eddies indicate that their
 157 momentum balance is very close to being geostrophic as we would have expected given their modest
 158 amplitude, Rossby number $R_o \leq 0.03$ (Sec. 5, Part 2), a horizontal scale greater than the radius of
 159 deformation, $L > R_d, R_d = C/f \approx 40$ km, and generally slow evolution compared to the rotation time,
 160 $1/f$. Highs and lows of SSH — anti-cyclones and cyclones — are about equally common.

161 **2) Geography and seasonality.** Mesoscale eddies are very widespread but their amplitude shows
 162 considerable spatial variability. The largest SSH amplitudes, up to about about ± 0.2 m, are found near
 163 the western boundaries of the subtropical and subpolar basins. Eddy amplitudes are considerably less in
 164 the eastern half of the subtropical North Atlantic, and mesoscale eddies are rather rare in the equatorial
 165 region, outside of the North Brazil current. There is very little evidence of seasonality of eddy amplitude
 166 or other properties, suggesting that direct forcing by the atmosphere is not the primary generation process
 167 (the equatorial region being a partial exception).

168 **3) Westward propagation.** Aside from regions having strong mean currents, e.g., the North Brazil
 169 current or the Gulf Stream and its extension into the subpolar gyre, mesoscale eddies propagate westward,
 170 slowly, but relentlessly. On average over all ocean basins, the eddy propagation speed at 30° latitude has
 171 been estimated from satellite altimetric data to be $3.5 \pm 1.5 \times 10^{-2}$ m sec⁻¹ or about 3 km day⁻¹. The
 172 observed eddy propagation speed decreases somewhat toward higher latitude, and increases markedly
 173 toward lower latitudes down to about 15° . At still lower latitudes, the SSH signature of mesoscale eddies
 174 is much reduced.¹

175 2.1 What's up with this β -plane?

176 We can begin to understand many of these observed properties by studying the evolution of a single eddy
 177 made by geostrophic adjustment, just as in Part 2, with the only new wrinkle being $f(\phi)$ given by Eqns.
 178 (2) and (3) vs. an f -plane in Part 2. As well, the integrations are continued for a much longer duration, up
 179 to a year. Everything that we saw and learned from the f -plane adjustment experiments in Part 2 will

¹A comprehensive analysis of mesoscale eddies observed in altimetric data is by Chelton, D.B., Schlax, M.G., Samelson, R.M., 2011, Global Observations of Nonlinear Mesoscale Eddies, *Progress in Oceanography*, doi: 10.1016/j.pcean.2011.01.002. Other recent analyses of the oceanic mesoscale are by Fu, L., D. B. Chelton, P. Le Traon and R. Morrow, 'Eddy dynamics from satellite altimetry', *Oceanography Mag.*, 2010, and by Zang, X. and C. Wunsch, 1999, *J. Phys. Oceanogr.*, 29, 2183-2199. Fu, L-L., 2009, 'Pattern and velocity propagation of the global ocean eddy variability', *J. Geophys-Res Oceans*, 114, C11017, doi:10.1029/2009JC005349 notes the often very large effect of the time-mean ocean circulation upon eddy propagation.

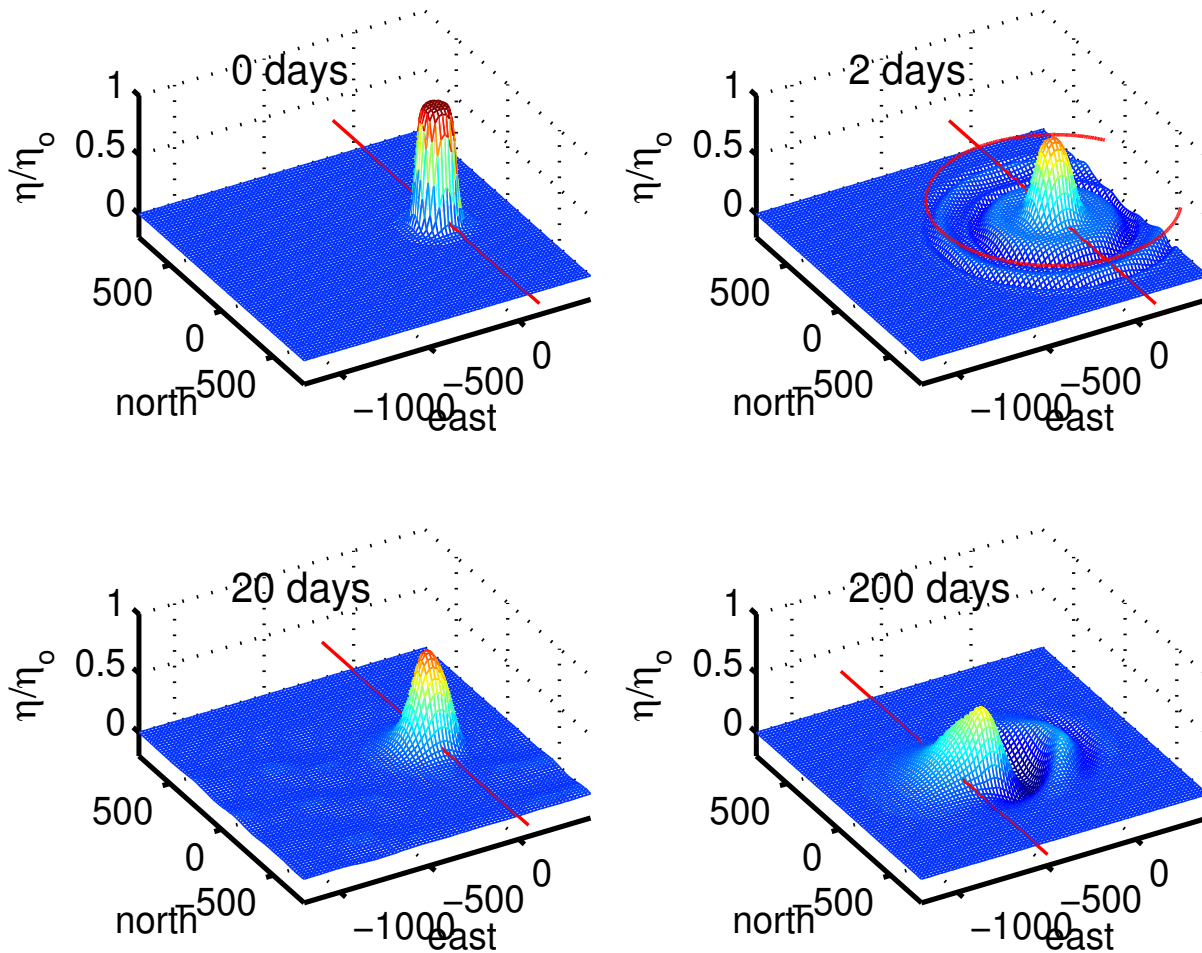


Figure 2: A numerical experiment in geostrophic adjustment on a β -plane solved by the numerical model `geoadj_2d.for`. The normalized anomaly of layer thickness, η/η_0 ($\eta_0 = 50$ m), is shown at four times: (upper left) the initial state of rest at $time = t = 0$, (upper right) 2 days after the eddy was released, and while inertia-gravity waves were prominent, (lower left) at 20 days, and (lower right) at 200 days, by which time the beta-induced westward propagation of the eddy peak is pronounced. The figures are annotated with a thin red circle having a radius $r = L + Ct$ that expands at the gravity wave speed, $C = \sqrt{g'H} \approx 300$ km day $^{-1}$ and so is off the model domain in about five days. There is also a thin red line oriented north-south that moves westward at the long Rossby wave speed, $-\beta R_d^2$, which is about 3 km day $^{-1}$ for this experiment (Sec. 2.3). It can be very helpful to see these data animated: www.whoi.edu/jpweb/pos50-h.flv

180 recur here, but alongside several new and very important phenomena — β -effects — that owe their
 181 existence to the inclusion of the β term in (2). The spatial domain of the model is two-dimensional, with
 182 (x, y) the east and north coordinates, and the domain is 3000 km on a side. The initial condition is taken
 183 to be a right cylinder of radius $L = 100$ km, and thickness anomaly, $\eta_0 = 50$ m. This corresponds to an
 184 SSH anomaly of about 0.1 m (from the reduced gravity approximation, Sec. 2, Part 2), which is typical of
 185 observed SSH mesoscale variability. The initial velocity is everywhere at rest. The initial eddy is thus a
 186 potential vorticity anomaly compared to the outlying fluid, i.e., inside the initial eddy, $q = f/(\eta_0 + H)$,
 187 while outside, $q = f/H$. Since these experiments start with a mesoscale eddy-sized q anomaly, the
 188 obvious, important question — why are there such thickness anomalies? — is deferred until considered
 189 very briefly in Sec. 2.5.

190 In the case of a mesoscale eddy having radius $L = 100$ km, the spatial variation of f is small,
 191 $\beta \delta y / f_0 = 2L/R_E \approx 0.03$, and so it is not surprising that the first few days of the geostrophic adjustment
 192 process are very similar to that seen in the f -plane experiments of Part 2, including, initially, isotropic
 193 radiation of inertia-gravity waves (Fig. 2). But after about a week, the inertia-gravity wave field develops
 194 a noticeable north-south asymmetry, Fig. (3). The waves that propagate poleward (northward in this case)
 195 are propagating toward higher f . Within a few thousand kilometers these waves reach a latitude at which
 196 their intrinsic frequency approaches f . Recall from Part 2 that free inertia-gravity waves can not exist at a
 197 latitude where their frequency is less than the local inertial frequency, f , and this is true on a β -plane as
 198 well. Poleward-traveling inertia-gravity waves are thus reflected equatorward. After about ten days have
 199 passed, the region that is poleward (northward) of the eddy is nearly free of inertia-gravity waves, while
 200 the equatorward side is still fairly energetic. This β -induced refraction of inertia-gravity waves is an
 201 interesting and important process of the ocean's internal wave sea state. However, the emphasis here is on
 202 low frequency phenomenon, and this particular β -effect will not be discussed further.

203 Over a longer period this experiment reveals a wholly new process that follows from the seemingly
 204 small change made to the Coriolis parameter — it (the eddy peak) moves due west at a slow but steady
 205 rate, -0.029 m sec⁻¹ or roughly 3 km per day. This westward propagation is significant in that it is 1) a
 206 robust and well-resolved feature of the numerical solution, and 2) closely comparable to the observed,
 207 westward propagation of ocean mesoscale eddies at this latitude (Fig. 1). Notice that the eddy peak just
 208 about keeps pace with the thin red line of Fig. (2) that is translated westward at the long Rossby wave
 209 speed appropriate to the present stratification and central latitude, $-\beta R_d^2 = -0.036$ m sec⁻¹, discussed in
 210 detail in Sec. 2.4.

211 The eddy peak in η remains well-defined, though the amplitude diminishes over time, especially at
 212 the beginning of the experiment. A spreading wake of decidedly wavy-looking ridges and troughs
 213 appears to trail behind the eddy peak, and eventually extends slightly eastward of the initial eastward
 214 edge, $x = 100$ km. The energy present in these waves must have come from the initial potential energy of

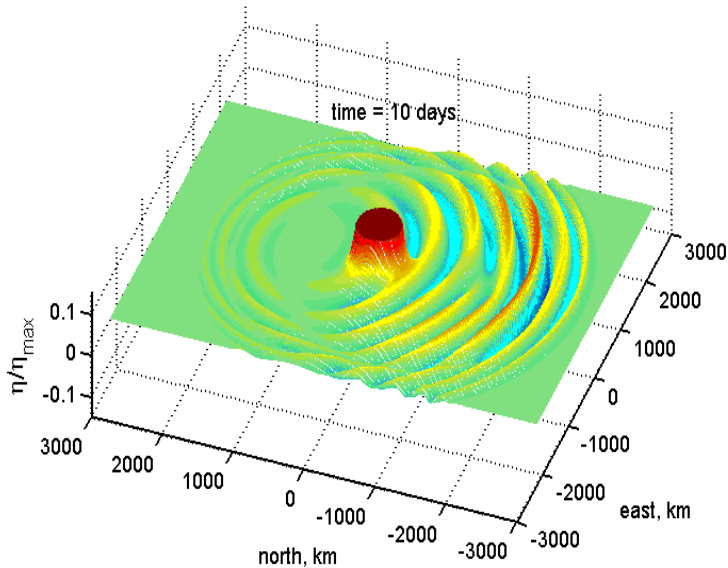


Figure 3: A snapshot of scaled thickness anomaly ($\eta_{max} = \eta_0 = 50$ m) 10 days after the start of a β -plane adjustment experiment. Poleward (north) is to the left in this figure. The vertical scale is severely truncated to emphasize the comparatively small amplitude inertia-gravity waves. By this time the wave amplitude is much reduced on the poleward side of the eddy. This north-south asymmetry in wave amplitude is due to a beta-induced reflection of the poleward-traveling, inertia-gravity waves. An animation of this data is: www.whoi.edu/jpweb/igwaves-beta.flv

215 the raised interface, and hence the spreading of energy away from the eddy peak is consistent with the
 216 decrease in the eddy peak amplitude.

217 The primary goals for the remainder of this section are to develop an understanding of the westward
 218 propagation of the eddy peak and the spreading (dispersion) of energy. The implicit assumption is that if
 219 we can understand these aspects of the numerical experiment, then we will have developed also a
 220 candidate understanding of the westward propagation of oceanic mesoscale eddies.²

221 2.2 Potential vorticity conservation

222 The westward propagation of the eddy peak seen in Fig. (2) is reminiscent of the propagation of the wave
 223 pulses of Sec. 3 Part 2 insofar as the eddy peak propagates steadily and as a somewhat coherent feature
 224 (though with appreciable decay discussed below). This westward propagation is very slow, however, only

²Westward propagation persists until the eddy peak reaches the western boundary of the computational domain. The subsequent evolution of the eddy depends entirely upon the boundary condition imposed on the western edge of the domain. The radiation boundary condition used here (Sec. 2.2, Part 2), $\partial(\cdot)/\partial t = -U_{rad}\partial(\cdot)/\partial x$ with $U_{rad} = C = \sqrt{g'H} = 3$ m sec⁻¹, is effective at minimizing the undesirable reflection of the fast-moving gravity waves. However, this comparatively large U_{rad} will act to push the eddy through the western boundary much more rapidly than it would otherwise go. Since the gravity wave and Rossby wave processes are so distinct in this experiment, it is sufficient to simply reset U_{rad} to the long Rossby wave speed, $U_{rad} = \beta R_d^2 \approx 0.03$ m sec⁻¹ (Sec. 2.2) after enough time has elapsed, 30 days.

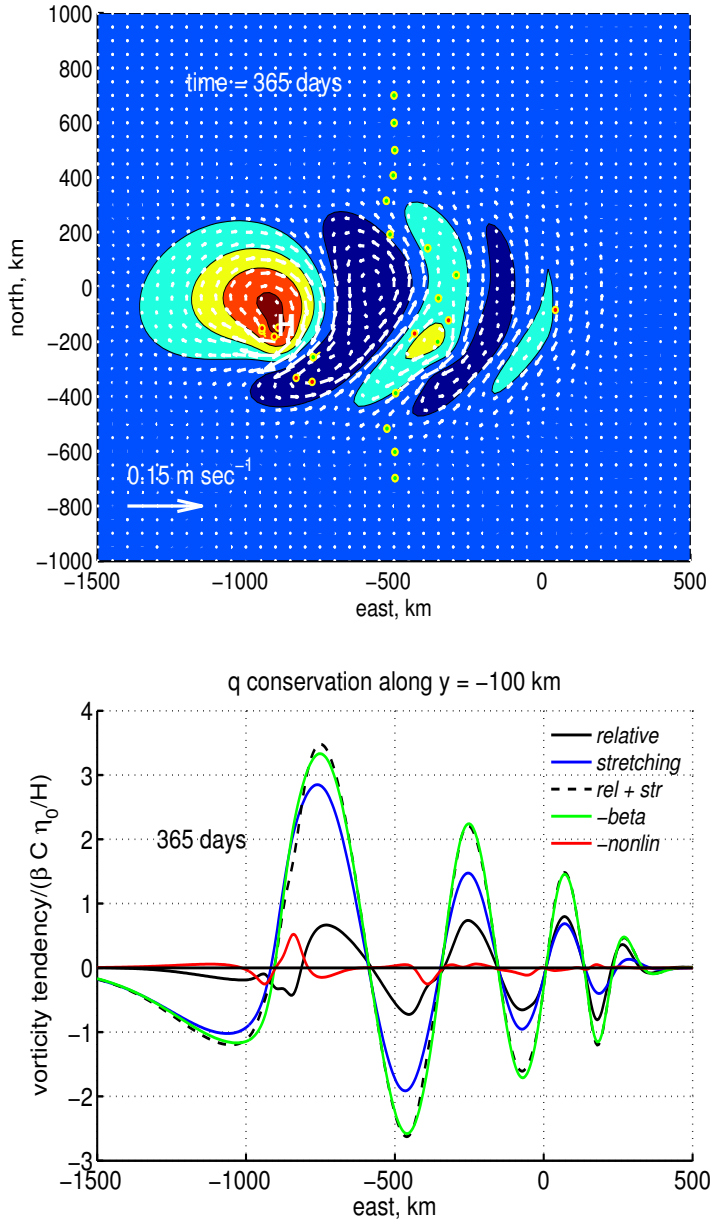


Figure 4: **(upper)** A snapshot of the horizontal velocity and thickness anomaly η (color contours, proportional to pressure) from the β -plane geostrophic adjustment experiment of Fig. (2). The north coordinate, y , was centered on 30°N ; the east coordinate, x , increases to the right. The big vector at lower left has a magnitude $0.5C\eta_0/H$ and serves as a scale for speed. This is a snapshot at 365 days; an animation is online at www.whoi.edu/jpweb/pos50-u.flv. The red and green dots are floats (passive fluid parcels) that will be discussed in Sec. 2.5. **(lower)** The potential vorticity balance (8) evaluated at $time = 365$ days along the line $y = -100$ km through the eddy peak in η . Here the β term has been moved to the right side of the equation, as *relative* + *stretching* = *-beta* - *nonlin* which helps show that (negative) *beta* term (green line) is closely balanced by the sum of the time rate of change of *relative* vorticity (black line) and vortex *stretching* (blue line; the sum *relative* + *stretching* is the black dashed line). Notice that the horizontal scale of the motion decreases from west to east, while the ratio *relative*/*stretching* (black/blue) increases from west to east. This systematic variation of horizontal scale and q -conservation mechanism is characteristic of a dispersing Rossby wave pulse discussed in Sec. 2.3.

225 about one percent of the gravity wave speed, C . At a fixed point, the time rate of change, and thus the
 226 frequency, ω , is correspondingly very low, about 1% of f . Is there a useful wave description of this
 227 westward propagation? The corresponding wave motion is certainly not contained within the f -plane
 228 model, since no free motion exists in the low frequency band $0 \leq \omega \leq f$ (Sec. 4, Part 2) and even more to
 229 the point, a balanced eddy stays where it is put on an f -plane (Sec. 5, Part 2). An analysis of westward
 230 propagation will evidently require taking explicit account of the one new feature of this experiment, the
 231 northward variation of f represented in Eqn. (2) by βy . The straightforward and appealing technique of
 232 looking for plane wave solutions directly in the governing equations (Sec. 4, Part 2) does not go through
 233 when $f = f(y)$ since the coefficients in the linear shallow water equations are then not constants.

234 How to proceed? Two clues: 1) In the shallow water model integrated here the potential vorticity
 235 should be conserved following parcels since there is no external forcing (and aside from real or
 236 inadvertent numerical diffusion). In that sense the conservation of potential vorticity is already known,

$$237 \quad \frac{Dq}{Dt} = \frac{D}{Dt} \left(\frac{\xi + f}{h} \right) = 0. \quad (5)$$

238 It remains to learn how the various terms of (5) achieve this balance, and doing so yields considerable
 239 insight into the mechanism of westward propagation (Sec. 2.4). 2) The velocity and pressure fields
 240 associated with the propagating eddy are transverse and nearly geostrophic; it is hard to see any
 241 discrepancy between the velocity direction and the local pressure isolines, though exact geostrophic
 242 momentum balance clearly can not hold. Nevertheless, geostrophy might be used to eliminate one of η or
 243 ξ and so to arrive at a governing equation for the slowly evolving, nearly geostrophic flow seen in this
 244 experiment.

245 The shallow water q -conservation equation (5) expanded and noting that $h = H + \eta$ and
 246 $Df/Dt = \partial f/\partial t + v\partial f/\partial y = \beta v$ is

$$247 \quad \frac{D\xi}{Dt} - \frac{D\eta}{Dt} \frac{\xi + f}{(H + \eta)} + \beta v = 0, \quad (6)$$

$$248 \quad \text{nonlin relative} + \text{nonlin stretching} + \text{beta} = 0.$$

250 The terms are the material time rate change of *relative* vorticity, the material time rate change of
 251 thickness, here called *vortex stretching*, and the very important *beta* effect due to meridional flow through
 252 a y -varying f . Since this D/Dt is the material derivative, the first two terms are nonlinear. As we will see
 253 shortly, the dominant terms for this experiment are three linear terms that are embedded in (6), and it is
 254 very helpful to sort them out. The important *beta* term is linear as is. The *nonlin relative* term is easily
 255 factored into a local time rate of change, which is linear, and an advection term that is nonlinear,

$$256 \quad \frac{D\xi}{Dt} = \frac{\partial \xi}{\partial t} + \mathbf{V} \cdot \nabla \xi.$$

257 The *nonlin stretching* term may be expanded into

$$258 \quad \frac{D\eta}{Dt} \frac{\xi + f}{(H + \eta)} = \frac{\partial\eta}{\partial t} \frac{f}{H} - \frac{\partial\eta}{\partial t} \frac{\eta f}{(H + \eta)^2} + \frac{\partial\eta}{\partial t} \frac{\xi}{H + \eta} + \mathbf{V} \cdot \nabla \eta \frac{\xi + f}{H + \eta}, \quad (7)$$

259 where the first term on the right side of (7) is linear and usually the largest term, and the next three terms
260 are all nonlinear. Substituting these expansions into (6) and collecting the linear terms on the left yields³

$$261 \quad \frac{\partial\xi}{\partial t} - \frac{f}{H} \frac{\partial\eta}{\partial t} + \beta v = -\mathbf{V} \cdot \nabla \xi + \frac{\partial\eta}{\partial t} \frac{\eta f}{(H + \eta)^2} - \frac{\partial\eta}{\partial t} \frac{\xi}{H + \eta} - \mathbf{V} \cdot \nabla \eta \frac{\xi + f}{H + \eta}, \quad (8)$$

262

$$263 \quad \text{relative} + \text{stretching} + \text{beta} = \quad \quad \quad - \text{nonlin.}$$

264 The terms of Eqn. (8) evaluated along an east-west slice through the eddy peak η , along $y = -100$
265 km, and for the *time* = 365 days are in Fig. (4), bottom. The nonlinear term (red line) is appreciable near
266 the eddy peak, but over most of the domain and including within the eddy, the β term is very nearly
267 balanced by the sum of the relative and stretching vorticity terms, which are in phase. Thus the q balance
268 of this phenomenon approximates the linear q balance,

$$269 \quad \boxed{\frac{\partial\xi}{\partial t} - \frac{f}{H} \frac{\partial\eta}{\partial t} + \beta v = 0} \quad (9)$$

$$\text{relative} + \text{stretching} + \text{beta} = 0.$$

270 Many of the large scale, low frequency phenomena of the atmosphere and ocean have a significant
271 overlap with this linear q -balance, even when, as here, they may also exhibit finite amplitude effects and
272 be subject to external forcing. The upcoming Sec. 2.3 will examine the free waves that are supported by
273 Eqn. (9), planetary Rossby waves, and finite amplitude (nonlinear) effects will be discussed in Sec. 2.4.

274 Assuming that the object will be motions having very low frequency, $\omega/f \ll 1$, and modest
275 amplitudes, $\eta/H \ll 1$, then the velocity and pressure will be nearly geostrophic. In that case the
276 geostrophic relations for north-south velocity, $v = (g'/f)\partial\eta/\partial x$, and vorticity, $\xi = (g'/f)\nabla^2\eta$, may be
277 substituted in to Eqn. (9) to eliminate the velocity components in favor of η . After a little rearrangement
278 there comes a linear, third order governing equation for η ,

$$279 \quad \left(\frac{g'H}{f^2}\nabla^2 - 1\right)\frac{\partial\eta}{\partial t} - \frac{\beta g'H}{f^2}\frac{\partial\eta}{\partial x} = 0, \quad (10)$$

280

281

$$\text{relative} + \text{stretching} + \text{beta} = 0.$$

³Notice that the dimension of these terms is *vorticity time*⁻¹, i.e., it is a vorticity tendency equation. Eqn. (6) will nevertheless be referred to as a *potential* vorticity conservation equation, since that was the essential origin.

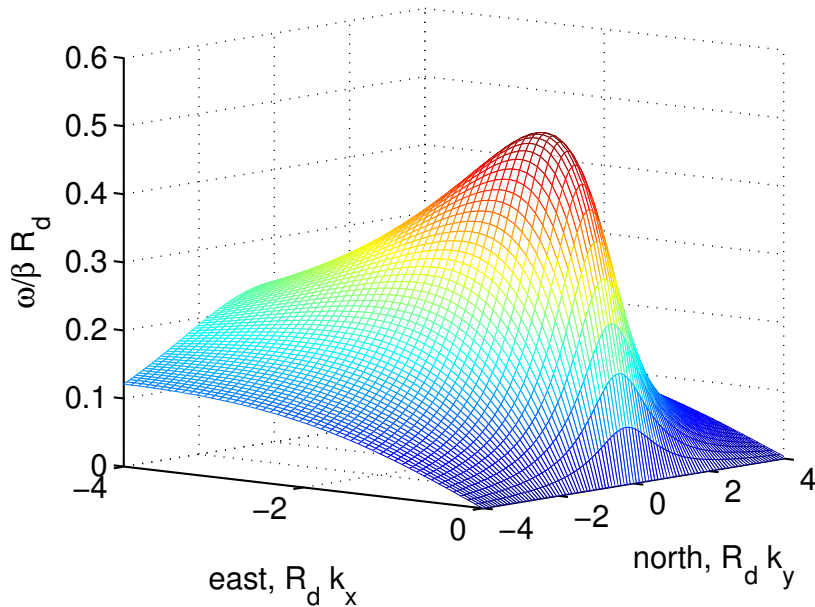


Figure 5: The dispersion relation for planetary Rossby waves, Eqn. (12). Frequency is normalized by $\beta R_d = 2\pi/85$ days, evaluated for a baroclinic midlatitude ocean. This surface is symmetric in the north-south component of the wavenumber vector, k_y . The east-west component can only be negative, i.e., $k_x < 0$ for planetary Rossby waves.

282 Notice that the time derivative of η is proportional to the first derivative of η in one direction, east-west.
 283 The dynamics of a β -plane is evidently anisotropic (not the same in all directions), which is a significant
 284 difference from an f -plane. This crucial dependence upon direction can be attributed to Earth's rotation
 285 vector (Part 1), which defines a specific direction for geophysical flow phenomena that are 1) low
 286 frequency enough to be significantly effected by the Coriolis force and 2) that have sufficiently large
 287 horizontal scale to be effected by the spatial variation of f due to Earth's nearly spherical shape.

288 2.3 Planetary Rossby waves

289 It is of considerable interest to learn how the balance of potential vorticity depends upon the horizontal
 290 spatial scales and the time scale of the motion. To learn the result for the important case of linear and
 291 nearly geostrophic potential vorticity, Eqn. (10), we need only substitute an elementary plane wave form,

$$292 \quad \eta(x, t) = \eta_0 \exp(i(k_x x + k_y y - \omega t)) \quad (11)$$

293 into Eqn. (10). A spatial derivative in the x direction thus brings out the east-west component of the
 294 wavenumber, k_x , and a partial time derivative brings out the frequency, ω (assumed to be positive in all

295 that follows). Solving for the frequency yields the dispersion relation for planetary Rossby waves,^{4,5} Fig.
296 (5),

$$\omega = -\beta R_d \left(\frac{R_d k_x}{1 + R_d^2 (k_x^2 + k_y^2)} \right) \quad (12)$$

298 Notice that as was the case for inertia-gravity waves, the dispersion relation depends upon the
299 stratification through R_d and Earth's rotation through f ; notably, this dispersion relation also depends
300 upon β .

301 The dispersion relation (12) is a very useful characterization of the linear, quasi-geostrophic vorticity
302 balance Eqn. (10) and will be discussed here at some length. However, it is worth noting that plane
303 Rossby waves — the literal interpretation of (11) — are generally *not* a prominent phenomena of the
304 oceans. For example, there are no plane (long-crested) Rossby waves evident in Fig. 1, though in other
305 years and other oceans, there may be, Sec. 2.6.2). Long-crested Rossby waves are not readily generated
306 by winds and other forcing mechanisms, which generally have shorter space scales, and, even when they
307 are, long-crested waves are likely to be unstable and evolve spontaneously into mesoscale eddies (an
308 example is in Sec. 2.5). The perspective on Rossby waves taken here is that while Rossby waves are
309 important in their own right, they are most important as the archetype of low frequency, nearly
310 geostrophic motions generally, and including mesoscale eddies. The dispersion relation (12) is our handy
311 guide to the relationship of time and space scales of such motions.

312 Rossby waves are altogether different from the inertia-gravity waves of Part 2. In the first place, they
313 have a very low frequency, and are very slowly moving; the factor in parentheses is $O(1)$ for the
314 wavenumbers and R_d of interest here and the frequency is determined largely by the leading factor,
315 $\beta R_d \approx f R_d / R_E$ which is $O(0.01)f$, when $R_d = 40$ km, appropriate to the subtropical baroclinic ocean.
316 This is the order of the frequency of both the numerical eddy and observed mesoscale eddies (Fig. 1).
317 The frequency of Rossby waves is strongly dependent upon the wavenumber vector, i.e., both the
318 magnitude and the direction. (This is in marked contrast to the isotropic dispersion relation of
319 inertia-gravity waves on an f -plane noted in Part 2.) The east-west component k_x must be negative and so

⁴An excellent all-around resource for oceanic Rossby waves is <http://www.noc.soton.ac.uk/JRD/SAT/Rosby/index.html>

⁵The terms 'eddy' and 'wave' are widely used, sometimes almost interchangeably. In fluid mechanics parlance, the most general use of 'eddy' is to denote any kind of departure from a spatial or a temporal mean. Here, eddy will be used to denote a flow feature having a quasi-circular planform and a thus more or less closed circulation. Mesoscale eddies are an example, and of course they are also a departure (anomaly) from a time or space average that would be appropriate for defining a basin-scale gyre. The term 'wave' might be applied reasonably to any phenomenon that results in the transmission of energy through a fluid (or solid) medium, though without necessarily transporting material. Mesoscale eddies on a beta-plane likely have just this property (Sec. 2.5) and so would qualify as waves in this (quite sensible) generalized sense. Here, however, the word 'wave' will be reserved here for an elementary plane motion of the sort Eqn. (11). Why this specific distinction between waves and eddies should be made clear in Sec. 2.7. (For a broad perspective on this issue see Scales, J. A. and R Sneider, 'What is a wave?', *Nature*, 401, 21 October, 1999, 739-740.)

320 planetary Rossby waves propagate phase to the west only. For a given wavenumber magnitude, the
 321 frequency is a maximum when the wave vector is directed due west, $k_y = 0$, and the frequency is zero if
 322 the wave vector is directed due north or due south, $k_x = 0$. In that case the currents are purely east-west or
 323 zonal, and hence not subject to a β -effect. Zero frequency implies steady and exactly geostrophic motion,
 324 and any purely zonal motion satisfies Eqn. (12) regardless of k_y . The dispersion relation (Fig. 5) is
 325 symmetric north-south, and the north-south component of phase velocity can have either sign. The
 326 east-west component of phase speed is always negative, i.e., always westward (Fig. 6), a fundamental
 327 property of planetary Rossby waves.

328 The numerical (and the real) mesoscale eddies propagate almost due west, and hence it is helpful to
 329 simplify the dispersion relation to the case of an east-west wave vector, i.e., $(k_x, k_y) = (k_x, 0)$, Fig. (6),

$$330 \quad \omega = -\beta R_d \left(\frac{R_d k_x}{1 + R_d^2 k_x^2} \right). \quad (13)$$

331 The phase speed in the east-west direction is

$$332 \quad C_p = \frac{\omega}{k_x} = -\beta R_d^2 \left(\frac{1}{1 + R_d^2 k_x^2} \right) \quad (14)$$

333 and always negative (westward). The maximum phase speed occurs with the longest waves, and is up to
 334 βR_d^2 , a stately 3 kilometers per day. The phase speed is, of course, a fundamental property of any wave,
 335 but nevertheless, the group speed is more evident in the experiments conducted here in which the waves
 336 spread from a confined region. The east-west group speed is

$$337 \quad C_g = \frac{\partial \omega}{\partial k_x} = -\beta R_d^2 \left(\frac{1}{1 + R_d^2 k_x^2} \right) \left(1 - 2 \frac{R_d^2 k_x^2}{1 + R_d^2 k_x^2} \right), \quad (15)$$

338 which may be written

$$339 \quad C_g = C_p \left(1 - 2 \frac{R_d^2 k_x^2}{1 + R_d^2 k_x^2} \right). \quad (16)$$

340 The group speed is westward for long waves, $R_d k_x \geq -1$, and also has a maximum magnitude of βR_d^2 .
 341 The phase and the group speed are proportional to β and so increase toward the equator. The group speed
 342 is eastward but rather slow even by Rossby wave standards for medium and short waves, $k_x R_d < 1$. The
 343 maximum eastward group speed is about $0.15 \beta R_d^2$, or only about 1/2 kilometer per day at mid-latitudes,
 344 and occurs at $R_d k_x = -\sqrt{3}$. There is clear evidence of this slow eastward energy propagation in the
 345 idealized experiments that follow, but admittedly it is hard to see evidence of it in the real ocean.

346 In the preliminary discussion of the q -balance of Fig. (4), lower, it was noted that the β term is
 347 nearly balanced by the in-phase sum of relative vorticity and stretching vorticity. The next issue is the

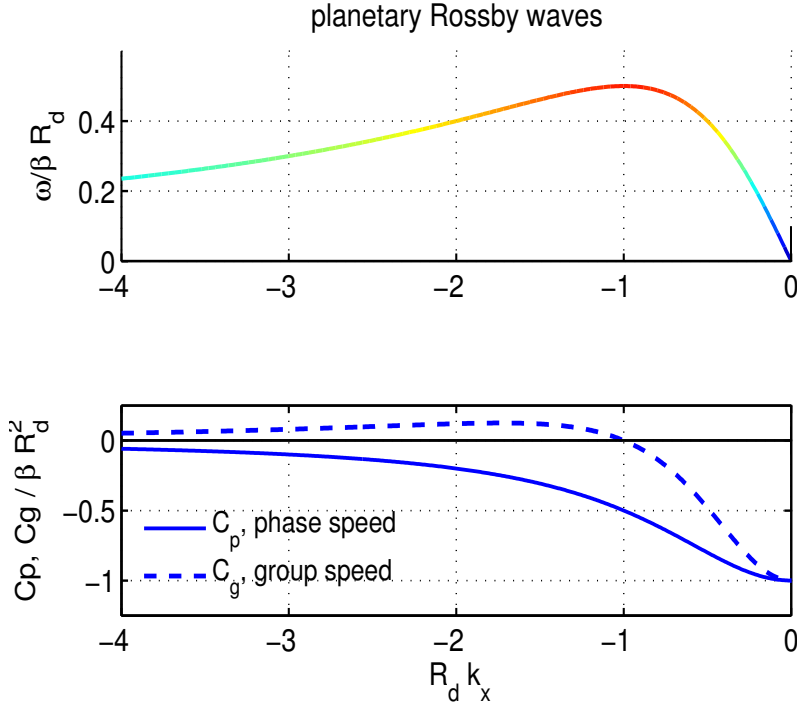


Figure 6: **(upper)** The dispersion relation for midlatitude, baroclinic, oceanic Rossby waves (Fig. 5) sliced along $k_y = 0$. Frequency is normalized by βR_d as before. **(lower)** Zonal phase and group speeds of planetary Rossby waves normalized by $\beta R_d^2 = 0.036 \text{ m sec}^{-1}$. The phase speed (solid line) is always negative, i.e., always westward. The group speed (dashed line) is also westward for long waves, $R_d k_x \geq -1$, and is eastward and small for medium to short waves, $R_d k_x \leq -1$.

348 ratio of these two terms and the correlation of the ratio with the horizontal scale of the motion and the
 349 east-west distance from the starting point. This may be estimated from Eqn. (10) using that ∇^2 operating
 350 on a plane wave $\propto \cos(k_x x - \omega t)$ gives $-k_x^2$ and thus,

$$351 \quad \frac{\text{relative}}{\text{stretching}} = \frac{\frac{g'H}{f^2} \frac{\partial \nabla^2 \eta}{\partial t}}{\frac{-\partial \eta}{\partial t}} = \frac{g'H}{f^2} k_x^2 = R_d^2 k_x^2. \quad (17)$$

352 Relative vorticity is thus more important for waves which have a short horizontal scale, i.e. $R_d k_x \gg 1$,
 353 while stretching vorticity dominates for longer waves, $R_d k_x \ll 1$. The eddy of our geostrophic adjustment
 354 experiment has an initial scale $R_d k_x \approx 1$, so that relative and stretching vorticity terms are comparable in
 355 the initial q balance. By 365 days, the eddy has dispersed, especially east to west, and the q -balance has
 356 become sorted out so that the ratio Eqn. (17) is about 4 in the vicinity of the eddy peak near $x = -1000$
 357 km, and the ratio is about 1/4 in the region around $x = 300$ km. The east-west scale of the motion also
 358 varies systematically, being considerably larger toward the west than in the east. This east-west variation
 359 of the q -balance and of the horizontal scale of the motion are consistent with the Rossby wave dispersion
 360 relation.

361 **2.3.1 Beta and relative vorticity; short Rossby waves**

362 The presence of a wave implies a restoring force that is related to the configuration of the system. In the
 363 common case of simple harmonic waves in a fluid or solid, the restoring force is proportional to the
 364 displacement of a parcel away from equilibrium. The restoring force of a gravity wave is straightforward
 365 — gravity acting upon a displaced sea surface or internal density interface. The restoring 'force' of a
 366 Rossby wave must be related to the presence of β and the north-south displacement of parcels in a
 367 y -varying f . The restoring force provided by the β -effect is somewhat indirect compared to gravity
 368 acting on a displaced density surface, but nevertheless results in two quite different mechanisms of
 369 westward propagation and two kinds of Rossby waves, short Rossby waves and long Rossby waves. To
 370 follow along with the discussion below it will be helpful for you to make sketches of
 371 $\eta(x, t) = \eta_o \cos(k_x x - \omega t)$, $v(x, t)$, etc., and fill in the very brief calculations outlined here.

Suppose that the motion (waves) is in the short wave limit $R_d k_x \gg 1$. If $R_d k_x = 5$, say, then for
 $R_d = 40$ km, $\lambda \approx 50$ km would suffice. In that case, the relative vorticity term is considerably greater
 than the stretching vorticity term and the conservation of q may be approximated by the conservation of
 absolute vorticity

$$\xi + f = \text{constant},$$

372 or in time-differentiated, linear form,

$$373 \quad \frac{\partial \xi}{\partial t} + \beta v = 0, \quad (18)$$

374 a balance between *relative* vorticity and *beta*. A northward meridional current, $v > 0$, thus induces a
 375 negative change in the relative vorticity, $\frac{\partial \xi}{\partial t} < 0$, and the converse for a southward meridional current.

To see the westward phase propagation that results from this q -mode, assume that the meridional
 velocity has the form of a propagating plane wave,

$$v(x, y, t) = V \cos(k_x x - \omega t),$$

376 with wavenumber directed due east-west. The zonal current then vanishes, and the relative vorticity is
 377 due solely to the east-west horizontal shear of the meridional velocity, $\xi = \partial v / \partial x$ (not the solid body
 378 rotation that is often depicted in qualitative diagrams, e.g., the spinning cylinder in Part 2, Fig. (4),
 379 middle). Substitution of this plane wave form into the reduced q -conservation equation (18) then yields

$$380 \quad \boxed{\omega = -\frac{\beta}{k_x}} \quad (19)$$

381 which is the short wavelength limit of Eqn. (14). The phase speed of short Rossby waves is then

$$382 \quad \boxed{C_{P_{shortRo}} = -\frac{\beta}{k_x^2}} \quad (20)$$

383 and westward. $C_{p_{shortRo}}$ is obviously dependent upon k_x so that short Rossby waves are highly dispersive.
 384 Their group speed is

$$385 \quad C_{g_{shortRo}} = \frac{\beta}{k_x^2} \quad (21)$$

386 and eastward, and notice equal in magnitude to the phase speed (Fig. 6).

387 The dispersion relation (19) is remarkable for what it omits: the dispersion relation (dynamics) of
 388 short Rossby waves does not depend upon the stratification or even the water column thickness; it
 389 depends only upon β and the zonal wavenumber, k_x . The motion is purely horizontal and nondivergent
 390 and so short Rossby waves are sometimes referred to as nondivergent Rossby waves. This is the
 391 q -conservation mechanism and the dispersion relation that C. G. Rossby inferred for westerly waves in
 392 the atmosphere (Secs. 1 and 2.6.1).

393 The group speed of short Rossby waves is very small, hundreds of meters per day as noted before, so
 394 that it takes quite some time for these waves to emerge from the initial eddy. But by day 365 there is clear
 395 evidence of slow, eastward energy propagation in the region $x > 200$ km (Fig. 4, lower). The horizontal
 396 scale in that easternmost region is, by inspection, $\lambda \approx 150$ km, and thus $R_d k_x \approx -2$, which is near the
 397 maximum eastward Cg . The linear q balance in that region is characterized by *relative/stretching* ≈ 4 .
 398 The very slow eastward extension of the eddy disturbance into the region east of the initial eddy position
 399 thus appears to be consistent with the slow eastward group speed and q balance of short(ish) Rossby
 400 waves.

401 2.3.2 Beta and vortex stretching; long Rossby waves

402 Another and very important mode of q -conservation holds for motions having a large horizontal scale in
 403 the sense that $R_d k_x \ll 1$. For the present case, $\lambda \geq 500$ km suffices. The change of relative vorticity is
 404 negligible for such large scale motions, and the q balance may be approximated as (Fig. 4, lower, Part 2)

$$405 \quad \frac{f}{H + \eta} = \text{constant}. \quad (22)$$

406 The linearized time rate of change is a balance between *beta* and vortex *stretching*,

$$407 \quad \beta v - \frac{f}{H} \frac{\partial \eta}{\partial t} = 0. \quad (23)$$

408 To see how this q -mode may support a wave, presume a zonally propagating thickness anomaly

$$409 \quad \eta(x, y, t) = \eta_0 \cos(k_x x - \omega t)$$

410 that is in geostrophic balance with a north-south (meridional) current,

$$411 \quad v(x, y, t) = \frac{g'}{f(y)} \frac{\partial \eta}{\partial x}.$$

412 Substitution into the reduced q -conservation equation and rearrangement yields

$$413 \quad \frac{\partial \eta}{\partial t} = \frac{g'H\beta}{f^2} \frac{\partial \eta}{\partial x},$$

414 a first order wave equation. Substitution of the presumed plane wave form yields the dispersion relation

$$415 \quad \boxed{\omega = -\beta \frac{g'H}{f^2} k_x} \quad (24)$$

416 the small $R_d k_x$ limit (i.e., the long Rossby wave limit) of Eqn. (14). The phase speed and the group speed
417 are the same,

$$418 \quad \boxed{C_{PlongRo} = C_{glongRo} = -\beta R_d^2} \quad (25)$$

419 and independent of k_x . Long Rossby waves are thus nondispersive.

420 The dispersion relation of long Rossby waves depends upon stratification. Because the
421 q -conservation mechanism of long Rossby waves is the β -induced divergence of the north-south (or
422 meridional) geostrophic current, long Rossby waves are sometimes called divergent Rossby waves.
423 Unlike the short Rossby wave, they can have a significant effect upon layer thickness, as we will see in
424 Sec. 4. Notice especially the crucial f^{-2} dependence of the long Rossby wave phase and group speed.
425 This will appear as a key, qualitative property at several junctures in this essay. An approximate
426 q -balance of this sort is evident in the vicinity of the eddy peak, $-1200 \leq x \leq -800$ km, where the
427 stretching term is about four times the magnitude of the relative vorticity term (Fig. 4, lower). The
428 wavelength is about $\lambda \approx 800$ km, and hence $R_d k_x \approx 0.3$, which is consistent with the ratio
429 relative/stretching. The eddy peak at 365 days thus has a horizontal scale that is near the non-dispersive
430 range of the Rossby wave dispersion relation (Fig. 6) and consistent with this, the eddy peak continues
431 propagating westward with little further change and at a rate, 80 to 90% of βR_d^2 , the long (Rossby) wave
432 speed.

433 Though the eddy peak certainly does not have the appearance of a plane wave, it nevertheless has the
434 q -balance and propagation characteristics of a (fairly) long elementary Rossby wave. Moreover, the
435 propagation speed of the numerical eddy is consistent with the observed speed of oceanic mesoscale
436 eddies at latitude 30° . Most importantly, the satellite altimetry observations of Fig. (1) allow this result to

437 be extended over a significant range of latitude.^{6,7}

438 2.4 Finite amplitude effects, and the dual identity of mesoscale eddies

439 To now our discussion of eddy phenomena has emphasized that linear Rossby wave theory gives a very
 440 useful account of the westward propagation and dispersion seen in the η and \mathbf{V} fields. This section will
 441 take a more in-depth look at the experiments and reveals two ways in which a linear description is
 442 incomplete: 1) First of all, there are modest but detectable finite amplitude effects on wave propagation in
 443 the base case experiment which has a realistic amplitude. 2) More striking is that fluid (tracer) transport
 444 by these eddies can be qualitatively different from the wave-like motion of the eddy peak and is entirely a
 445 finite amplitude effect. In this respect, mesoscale eddies have a kind of dual identity — Rossby wave-like
 446 when viewed in the η field, and yet capable of transporting tracer for significant distances depending
 447 upon amplitude. To highlight these phenomena and their dependence upon amplitude, it is helpful to
 448 compare the solutions from two new experiments made by setting the initial amplitude very small, $\eta_o = 1$
 449 m (Fig. 7), so that all finite amplitude effects should vanish, and then much larger, $\eta_o = 100$ m (Fig. 8),
 450 so that finite amplitude effects should be fairly pronounced.⁸

451 2.4.1 Eddy propagation seen in the η and \mathbf{V} fields

452 The overall appearance of the normalized interface displacement $\eta(x, y, t)/\eta_o$ and the normalized current
 453 $\mathbf{V}/(C\eta_o/H)$ are not greatly different between these two experiments, but there are differences in detail.
 454 Most notably, the amplitude of the eddy peak is preserved somewhat longer in the large amplitude

⁶A recent, comprehensive modelling study of the SSH climatology is by Early, J. J., R. M. Samelson and D. B. Chelton, 2011, 'The evolution and propagation of quasigeostrophic ocean eddies', *J. Phys. Oceanogr.*, doi: 10.1175/2011JPO4601.1 and references therein. Also highly recommended is <http://jeffreyearly.com/science/qg-eddies-paper/> A notable, early theoretical/numerical study is by McWilliams, J. C. and G. R. Flierl, 1979, 'On the evolution of isolated, nonlinear vortices', *J. Phys. Oceanogr.*, 9, 1155-1182. A collection of research reviews is by Hect, M. W. and Hasumi, H., 2008, 'Ocean modelling in an eddying regime', *Geophys. Mono. Ser.*, 177, American Geophys. Union.

⁷The discussion here was organized around two of the three modes of the linear potential vorticity balance that correspond with limits of the Rossby wave dispersion relation. Just to be complete, the third mode of vorticity balance is between stretching and relative vorticity, as in Fig. (4), upper, Part 2. In this mode, a change in relative vorticity occurs in phase with stretching, and thus when stretching stops, so does the change of relative vorticity. There is no mechanism for wave propagation associated with this mode, but it makes an important appearance in several numerical experiments; the geostrophic jets of Sec. 4.4, Part 2 exhibit this mode of q conservation, and there will be another example in Sec. 3.3 associated with Kelvin waves.

⁸This takes a short-cut. By the present definition of finite amplitude (Part 2, Sec. 2.3.4) we should first verify that there is indeed a linear regime at small amplitude by comparing the solutions from two (putatively) small amplitude experiments, say $\eta_o = 1$ m with $\eta_o = 2$ m, to verify that the scaled η s and \mathbf{V} s are indistinguishable. They are.

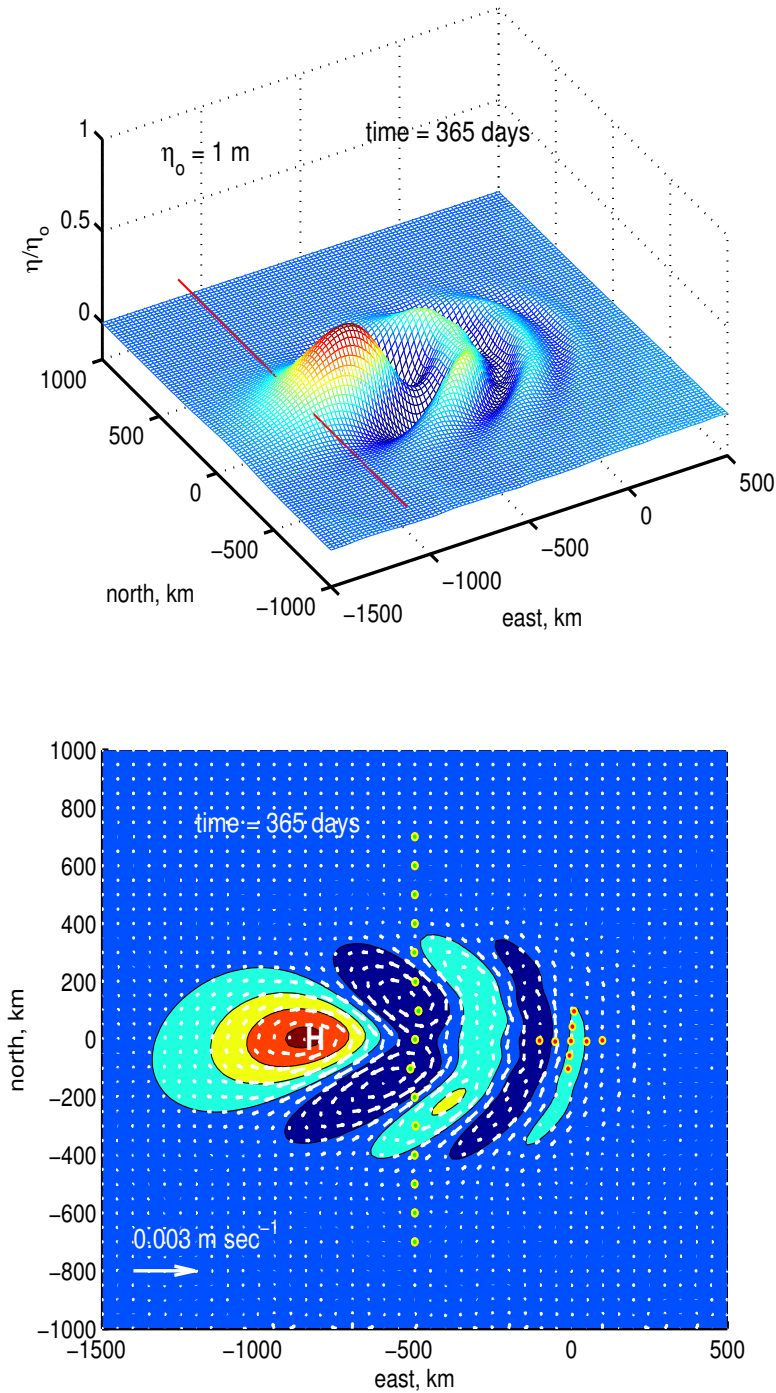


Figure 7: A small amplitude experiment in which $\eta_0 = 1 \text{ m}$ and $\eta_0/H = 0.002$ so that finite amplitude effects are negligible (a large amplitude experiment is next). **(upper)** The normalized interface displacement $\eta(x, y, t)/\eta_0$. **(lower)** The velocity field (vectors), thickness (color contours) and floats (red and green dots). The big vector at lower left has a magnitude $0.5C\eta_0/H$ and serves as scale for the velocity. The red floats were started within the eddy, while the green floats were set on a north-south line at $x = -500 \text{ km}$ and well to the west of the initial eddy. None of the floats moved an appreciable distance during the course of this year-long experiment, while the eddy peak propagated westward as if a linear wave. An animation of these data is available at www.whoi.edu/jpweb/pos1-u.flv

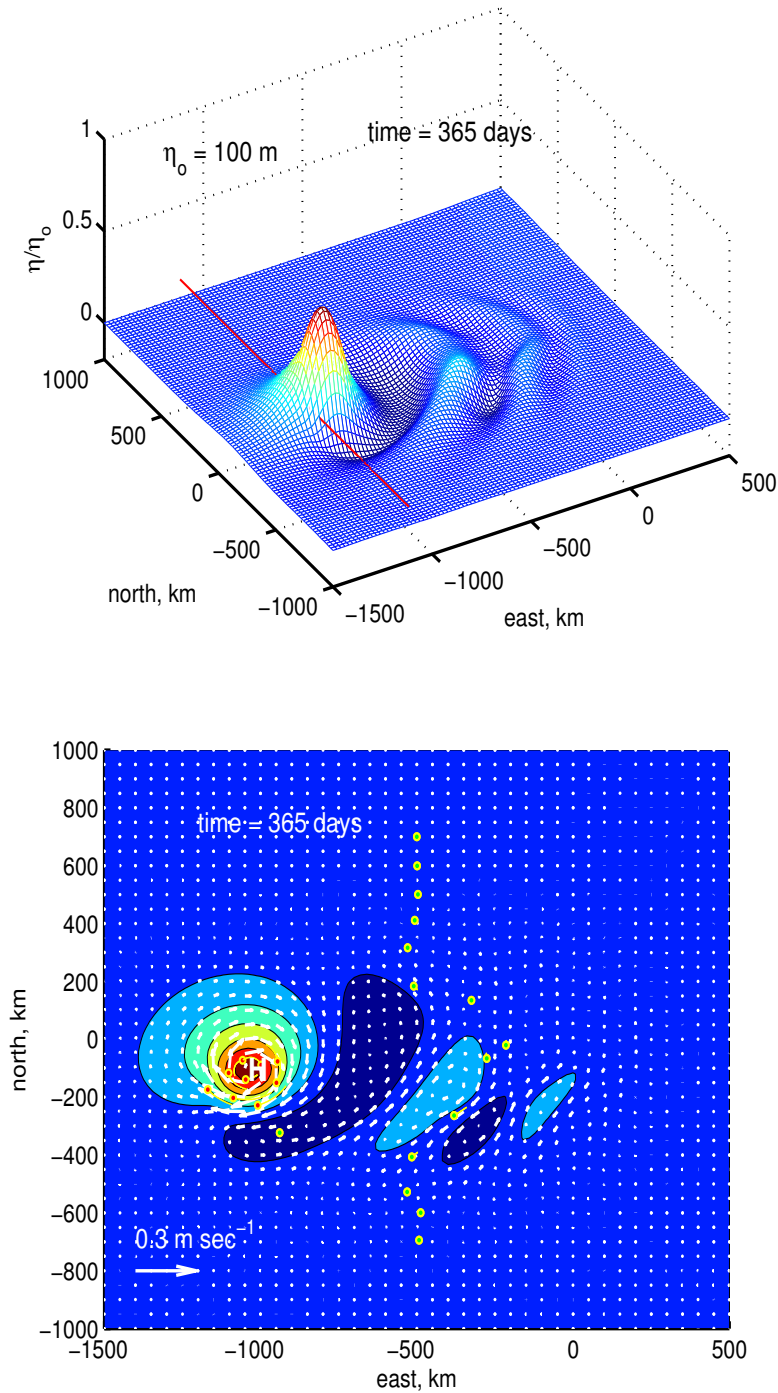


Figure 8: A large amplitude experiment, $\eta_0 = 100$ m and $\eta_0/H = 0.2$ so that finite amplitude effects are appreciable. **(upper)** Compared with the previous, small-amplitude experiment, Fig. (7), the (normalized) $\eta(x, y, t)$ eddy peak retained a somewhat larger fraction of its initial value. **(lower)** The velocity field and the floats of the large amplitude experiment. As before, the big vector at lower left has a magnitude $0.5C\eta_0/H$ and serves as the scale for velocity. The red floats, which were started within the eddy, were trapped by the eddy for the year-long duration of this experiment. The green floats, which were started well outside of the eddy along a north-south line at $x = -500$ km, were displaced mainly to the east as the eddy propagated by their initial longitude. The qualitative difference in these float trajectories compared to those of Fig. (7) shows that tracer (float) transport is a finite amplitude phenomenon. The animations provide a much more vivid sense of the differences between this and the previous experiment; this one is at www.whoi.edu/jpweb/pos100-u.flv

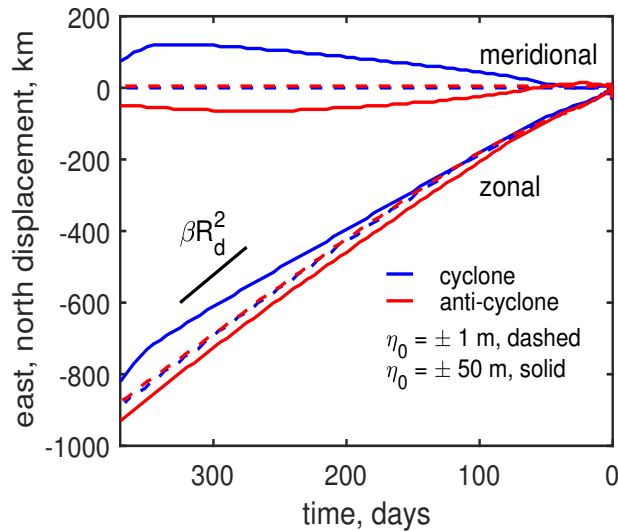


Figure 9: Time series of northward (here, poleward) and eastward displacement of the eddy peak (the maximum of $|\eta|$) for four experiments in which the amplitude and the sign of the initial displacement was $\eta_0 = \pm 1$ m (two dashed lines that are almost identical) or ± 50 m (the solid red and blue lines). Blue curves are from the cyclones and red curves are from anti-cyclones. In all cases the zonal displacement is dominantly westward and at about 80 to 90% of the long Rossby wave speed, βR_d^2 , evaluated at 30°N . The strong cyclone (solid blue line) shows a small meridional poleward displacement (upper set of curves), while the strong anti-cyclone (solid red line) shows a small meridional equatorward displacement.

455 experiment and the waves found to the east of the peak have less symmetry when compared to the small
 456 amplitude experiment.

457 The zonal propagation speed of the eddy peak is also altered by finite amplitude effects: the zonal
 458 eddy peak speed is about 80% of $C_{longRo} = -\beta R_d^2$ in the small amplitude experiment (Fig. 9, dashed
 459 lines, and Fig. 10) and is about 90% of C_{longRo} in a large amplitude experiment, $\eta_0/H = 0.2$. For still
 460 larger amplitudes there is little further increase and so it appears that the long Rossby wave speed is a
 461 speed limit for the zonal motion of these eddies.

462 Finite amplitude effects cause a noticeable meridional motion of the eddy peak. Large amplitude
 463 anti-cyclones ($\eta_0/H = 0.1$, solid red line of Fig. 9) show a small component of motion toward the
 464 equator, about 10% of the westward propagation speed. Large amplitude cyclonic eddies show a similar
 465 poleward motion (the solid blue line of Fig. 9). These modest but detectable finite amplitude effects on
 466 the speed and direction of the eddy propagation seen in η are consistent with the observed propagation of
 467 oceanic mesoscale eddies seen in SSH (Fig. 1).⁶

468 2.4.2 Fluid transport seen in tracer fields and float trajectories

469 There is another very important class of eddy phenomena, the long term transport of fluid, often called
 470 the Lagrangian velocity, Part 2 Sec. 2, that is strongly dependent upon eddy amplitude. To see the fluid

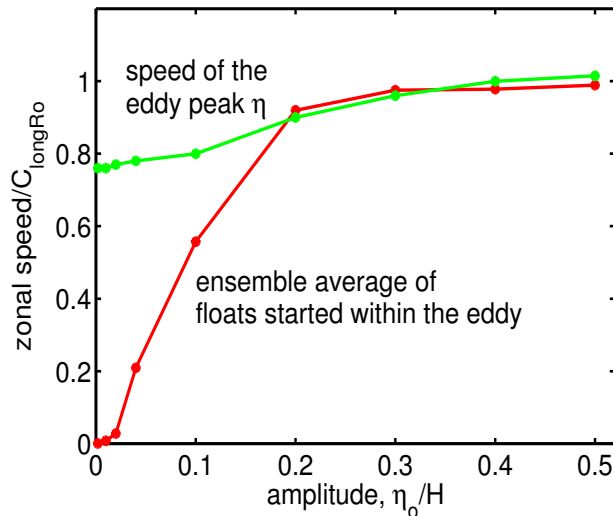


Figure 10: Average zonal speed of the eddy peak of η (green line; all anticyclones) and of an ensemble of floats that were launched within the eddy (red line) for nine experiments having amplitude $0.001 < \eta_o/H < 0.5$, the independent variable. The average is over the first year of the experiment. Speeds are normalized by the long Rossby wave speed at the average latitude of the eddy peak. The normalized eddy peak speed depends somewhat upon the eddy amplitude, while the ensemble-averaged float speed is very sensitive to eddy amplitude up to $\eta_o/H \approx 0.2$. These are robust results in a numerical solution sense, and an interesting comparison of two important properties of (numerical) mesoscale eddies. However, the eddy peak speed and the ensemble-averaged float speed (or Lagrangian velocity) are, in general, qualitatively different things, e.g., the float speed depends upon the averaging interval in the intermediate amplitude cases in which some fraction of the floats is lost from the eddy during the first year (as in Fig. 4, upper).

471 motion we have to analyze a tracer field or compute the trajectories of floats (passive particles). It was
 472 noted in Part 2 that the ideal (no external forcing) shallow water model has a natural, built-in tracer, the
 473 field of potential vorticity, q , which follows a conservation law, $Dq/Dt = 0$, i.e., q is conserved on fluid
 474 parcels. The initial condition on q (Fig. 11, left) in these experiments is a uniformly sloping background
 475 due to the northward increase of f , and a circular, low- q anomaly centered on $(x, y) = (0, 0)$ that is the
 476 initial (thick) eddy. It is interesting to solve in parallel for the evolution of a passive tracer, $Ds/Dt = 0$,
 477 whose initial condition can be set arbitrarily; one simple choice is $s_o = 1$ inside the radius of the initial
 478 eddy, and zero otherwise (Fig. 12, left). The motion of the eddy center is readily apparent in the
 479 evolution of either of these tracer fields and is exactly the same in these two fields, as it should be. In the
 480 base case experiment, which has a fairly large amplitude, $\eta_o/H = 0.1$, the q or s anomaly moves mainly
 481 westward and slightly southward, very much like the eddy peak in this experiment. It bears emphasis that
 482 the tracer and the eddy q anomaly can move only by virtue of the fluid motion (not wave motion). Thus
 483 the appearance of the eddy's low q anomaly is associated with a noticeable contribution by the *nonlin*
 484 term to q conservation (Fig. 4, lower). The main contribution to *nonlin* is from horizontal advection of

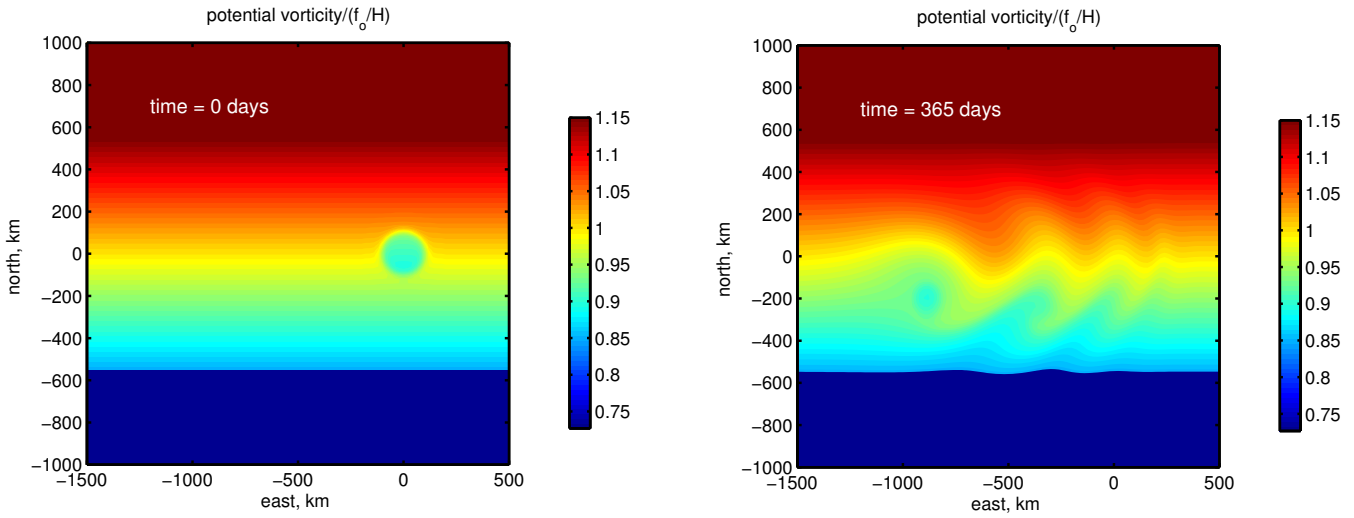


Figure 11: Potential vorticity from the experiment $\eta_o = 50$ m. **(left)** The initial condition. The eddy is the pale blue, low q anomaly centered on $(x, y) = (0, 0)$. **(right)** At 365 days. The eddy center marked by the potential vorticity anomaly is now at $(x, y) = (-900, -200)$ km, which is about 100 km equatorward of the eddy peak seen in η at this time.

485 relative vorticity (the first term on the right side of Eqn. (8)).

486 The background (non-eddy) parts of these two tracer fields are somewhat different. The q field at the
 487 latitude of the eddy shows rather large meridional displacements of constant q lines. The passive tracer
 488 shows something similar only where there happens to be a meridional tracer gradient, near the eddy
 489 center and in a long, thin filament of tracer that extends from the eddy center back toward the starting
 490 location. This loss of tracer from the eddy into the filament is accompanied by a slow decrease of the
 491 eddy radius, mainly. The same filament is present also in the q field, although not apparent against the
 492 background of Fig. (11).⁹

493 Fluid motion may be easier to quantify when diagnosed from the motion of discrete, passive parcels,

⁹This tracer filament is very interesting insofar as it may show how discrete eddies may act to disperse tracer properties. However, this filament is also just the kind of thing that is especially challenging for a numerical solution. Specifically, the width of the numerical filament (i.e., the filament within a numerical solution) can never be less than several times the horizontal grid interval, 5 km, which may be considerably greater than the natural, physical horizontal scale of the filament. Small changes in the diffusion (deliberate or numerical) or even in the method used to estimate and time-step the advection terms of the tracer equation can thus cause a significant difference in the width of the filament and thus in the tracer concentration along the filament, even while leaving the eddy propagation almost unaffected. Eddy propagation thus appears to be a robust and well-resolved process in these numerical solutions, while the width and tracer concentration along this very thin tracer filament are not.

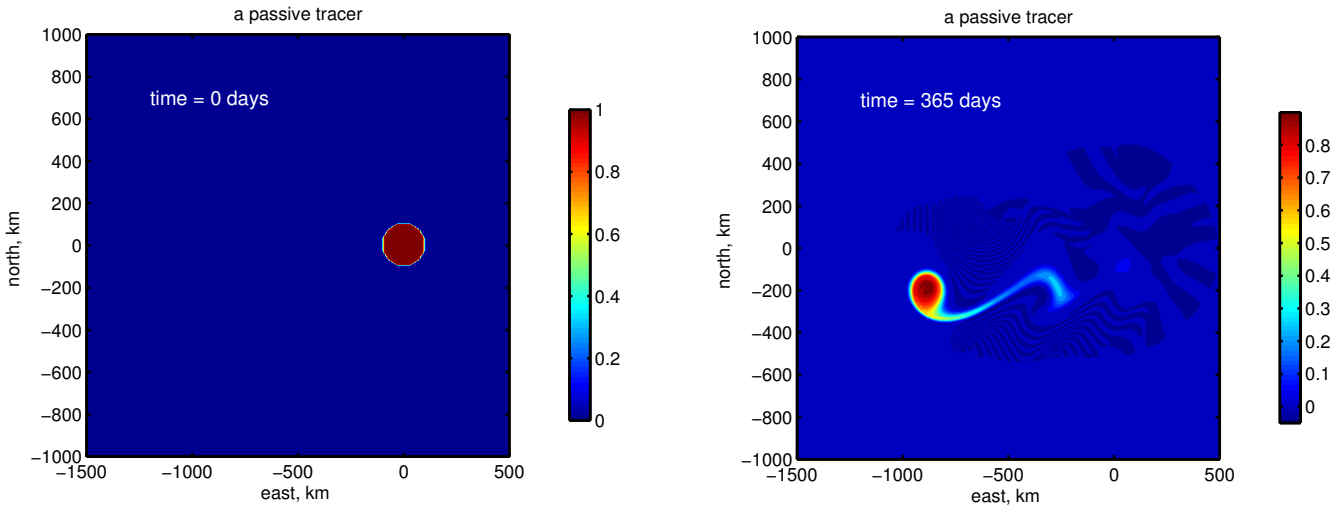


Figure 12: The evolution of a passive tracer inserted into the experiment $\eta_o = 50$ m. **(left)** The initial condition; $s = 1$ within the initial eddy, $s = 0$ otherwise. **(right)** At 365 days. Notice that the eddy center marked by tracer is at about $(x, y) = (-900, -200)$ km, and the same as seen in the q field of the previous figure. Notice too the thin, wispy trail of tracer left behind the westward-propagating eddy. This corresponds with the line of (red) floats dropped off by the eddy Fig. (4, upper) and with a faint local minimum of potential vorticity.

494 or 'floats' (Sec. 2.3.3, Part 2), that are set in the initial state. A cluster of nine (red) floats was started
 495 within the eddy to serve as a tag on the eddy, and a line of (green) floats was placed along a north-south
 496 line 500 km west of the eddy initial position (Fig. 7, lower) to show the motion of the ambient fluid as the
 497 eddy passes through their longitude. In the small amplitude experiment, $\eta_o/H = 0.002$ (Fig. 7), all of
 498 these floats appear to be essentially frozen in space for the full duration of the experiment. At the same
 499 time, the eddy marked by η moves westward as would a linear Rossby wave. The ensemble average
 500 speed of the red floats launched within the eddy is thus about zero, while the eddy peak defined by η
 501 propagates at about 80% of C_{longRo} . This qualitative difference between float (and thus fluid) motion and
 502 the motion of the eddy peak seen in η also leads to the depiction of the eddy peak motion as
 503 'propagation', and implicitly, wave propagation.

504 The float movement (and the transport of tracers and fluid) is very different in the large amplitude
 505 experiment, $\eta_o/H = 0.2$, (Fig. 8, lower), even while the westward propagation of the eddy peak is
 506 changed only slightly. The large amplitude azimuthal current within the eddy effectively traps the red
 507 floats on the side of the eddy where the current is westward, in the direction of the eddy propagation (the
 508 south side of the anticyclone of Fig. (8, lower). The eddy then advects the floats to the west-southwest
 509 over a distance of almost 1000 km within the first year. The long-term, ensemble mean Lagrangian
 510 velocity of these specific floats is thus the same as the speed of the eddy peak (Fig. 10), about 95% of

511 C_{longRo} . In an intermediate amplitude experiment, roughly $0.03 \leq \eta_o/H \leq 0.2$, e.g., Fig. (4, upper), some
 512 fraction of the red floats are lost from the eddy as it shrinks in radius during the first year, and hence the
 513 ensemble-average float speed is intermediate between 0 and the eddy peak speed. The ensemble-average
 514 float speed thus depends entirely upon the residence time of the floats within the eddy, which in turn
 515 depends upon the initial amplitude of the eddy and the rate at which it decays and disperses. This
 516 significant dependence of the float speed with amplitude fits the present definition of a finite amplitude
 517 phenomenon.¹⁰

518 2.5 Rossby waves \rightarrow Eddies

519 This essay has discussed Rossby waves (elementary, plane Rossby waves) and mesoscale eddies on a
 520 more or less equal footing. This may have left you wondering if these phenomenon are equally important
 521 and whether there may be connections between them, even aside from their common vorticity balance.
 522 One interesting connection is that under common circumstances, Rossby waves are expected to evolve
 523 spontaneously into mesoscale eddies, i.e., Rossby waves are very often unstable. The topic of fluid flow
 524 instabilities is beyond the scope of this essay, but a simple example of Rossby wave instability will serve
 525 to illustrate the phenomenon and (ideally) may stoke your appetite for more.¹¹

526 The model is initialized with a rather special state: a north-south oriented ridge/trough that mimics
 527 one isolated wave,

$$528 \quad \eta(x, y, t = 0) = \eta_o \frac{f}{f_o} \sin(2\pi x/\lambda) \quad \text{if } |x| < \lambda/2, \quad (26)$$

529 and otherwise

$$530 \quad \eta(x, y, t = 0) = 0 \quad \text{if } |x| > \lambda/2.$$

531 The wavelength is $\lambda = 600$ km. The currents are initialized with the corresponding geostrophic velocity.
 532 The evolution of this system is dependent upon amplitude, and so it is desirable to make the initial current

¹⁰The meridional drift of large amplitude eddies has been studied extensively in the context of tropical cyclone motion, see <http://www.aoml.noaa.gov/general/WWW000/nhurr00.html#mo>. In brief, the present eddies have a horizontal scale $KR_d \leq 1$ that is not completely large scale, i.e., the beta effect is not balanced solely by divergence. There is some relative vorticity generated by the meridional velocity of the eddy and an induced cyclonic vorticity on the northeast side of the eddy and cyclonic vorticity on the southwest side. The net result is a markedly asymmetric velocity field with a strong southwest current on the southern side of the eddy, readily evident in Fig. 8, bottom. This current acts to self-advect the eddy center toward the southwest. For a large amplitude cyclone the strongest current is on the northeast quadrant and is directed northwest. The amplitude of this current is much, much greater than the resulting southwest drift of an anti-cyclonic eddy (noted in the discussion above), evidently because it is on the periphery of the eddy, and is directed mainly along lines of constant h .

¹¹See Isachsen, P. E., J. H LaCasce and J. Pedlosky, 'Rossby wave instability and apparent phase speeds in large ocean basins', *J. Phys. Oceanogr.*, 2007, 1177-1191, DOI: 10.1175/JPO3054.1 and references therein.

533 the same at all latitudes. The amplitude was therefore scaled with f/f_o , with f_o appropriate to 30°N . In
 534 the first experiment the amplitude is very small, $\eta_o = 1$ m and thus $\eta_o/H = 0.002$; in a second
 535 experiment the amplitude is very large, $\eta_o = 100$ m and thus $\eta_o/H = 0.2$. In an attempt to minimize the
 536 effect of northern and southern boundaries of the model domain, the amplitude was tapered to zero
 537 approaching the equator and also at very high latitude (off of the model domain shown here).

538 Once this feature is released onto a β -plane we would expect westward propagation as a (fairly)
 539 long Rossby wave, and indeed that happens. There is quite noticeable dispersion since the isolated
 540 sinusoid Eqn. (26) is not a pure harmonic. As well, while the initial wavelength is long, $kR_d \approx 0.4$, it is
 541 not extremely so. When the initial amplitude is very small, $\eta_o/H \ll 1$, (middle panel of Fig. 13), the
 542 wave remains easily identifiable for $O(1000)$ days and the leading edge just about keeps pace with the
 543 expected long Rossby wave speed. When the amplitude is very large, $\eta_o/H = 0.2$ (lower panel of Fig.
 544 13), the evolution is dramatically different. Within a few hundred days there appears a semi-regular train
 545 of lumps and bumps along the length of the wave, and by about 500 days the original long-crested wave
 546 evolves into a semi-regular array of mesoscale eddies. These eddies have a scale (diameter) of about 250
 547 km in the northern (high latitude) portion of the domain, and somewhat larger, about 400 km in the low
 548 latitude part of the domain. These eddies are in the small wavenumber region of kR_d space, and so they
 549 too propagate westward at a rate that is just slightly less than the initial Rossby wave propagation. Even
 550 though the initially smooth and continuous wave breaks up rather dramatically, westward propagation
 551 nevertheless continues almost unabated.

552 The details of when and where the eddies form in this experiment depends sensitively upon the way
 553 that the initial wave is perturbed. Here the perturbation results mainly from the low latitude end of the
 554 wave, which recall was tapered to fit into the model domain. The real ocean is filled with all manner of
 555 perturbations having a wide range of time and space scales, though probably nothing quite like the
 556 tapering employed here. In any event, the result of the instability — mesoscale eddies — is not sensitive
 557 to the form of the perturbation.

558 Theory (see Isachsen et al.¹¹) indicates that the scale of the most rapidly growing instability is
 559 proportional to the local radius of deformation, consistent with the y -dependent diameter of the mature
 560 eddies found here. The rate at which the instability grows (once triggered by some kind of perturbation)
 561 is expected to be proportional to the amplitude of the initial wave. The two cases of Fig. (13) are extreme,
 562 $\eta_o = 1$ m and $\eta_o = 100$ m. In the former case the growth is so slow that there is little evidence of eddy
 563 formation even after almost two years. However, in the large amplitude case, which is closer to being
 564 realistic of the ocean, the growth is fairly fast, with eddies becoming apparent within several hundred
 565 days of the start of the experiment.

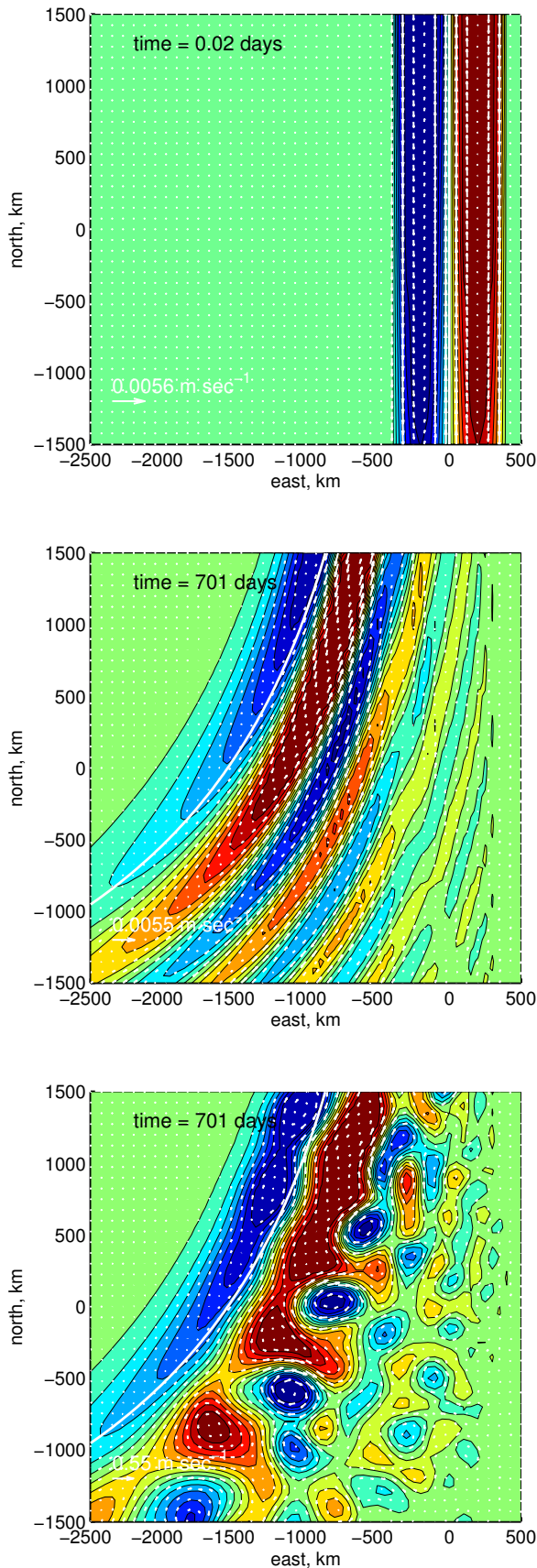


Figure 13: Two experiments that were initialized with a single meridionally-oriented wave in geostrophic balance. **(upper)** The initial condition. **(middle)** The normalized thickness anomaly and currents of a small amplitude case that had $\eta_o = 1 \text{ m}$. The white parabola was started at $x = 0$ and then displaced westward at the y -dependent long Rossby wave speed. The leading ridge/trough just about keep pace with this westward speed but there is also significant dispersion, with shorter wavelengths lagging well behind. **(lower)** A large amplitude experiment having $\eta_o = 100 \text{ m}$.

566 2.6 Some of the varieties of Rossby wave-like phenomenon

567 2.6.1 Westerly waves

568 The westerly wind belts that encircle the mid-latitudes in both hemispheres are nearly always perturbed
 569 by wave-like undulations, appropriately termed westerly waves, that are a very significant factor in the
 570 day-to-day variation of weather (Fig. 1, Part 1). The longest such waves having wavelengths of $O(10,000$
 571 $\text{km})$ are often observed to be almost stationary with respect to Earth despite that they are embedded in the
 572 eastward flowing westerly wind belt where the spatially-averaged wind is
 573 $\bar{U} \approx 30 \text{ m s}^{-1}$. The longest waves have a westward propagation speed that is just sufficient to stem this
 574 eastward advection and may appear to be nearly stationary with respect to the Earth. Quasi-stationary
 575 waves of this sort are very common in fluid flows around fixed obstacles: 'rapids' on the surface of a river
 576 and ripples on the flow of water from a faucet are familiar examples.

577 On the other hand, the shortest westerly waves, which may dominate the instantaneous pattern of the
 578 westerlies at other times (the web site noted in footnote 3, Part 1 shows instances of this) clearly
 579 propagate from west to east. In some cases short waves move eastward at a speed that is not much less
 580 than \bar{U} . Short westerly waves (which have wavelengths of several thousand kilometers) thus appear to be
 581 almost passively advected by the westerly wind. Rossby proposed that westerly waves propagate zonally
 582 within a zonal mean flow, \bar{U} , as

$$583 \quad C_w = \bar{U} - \frac{\beta}{k_x^2}, \quad (27)$$

584 which is the short (non-divergent) limit of the Rossby wave dispersion relation Eqn. (12) plus advection.
 585 This relation, and the analysis that led to it, proved to have great merit both as a fundamental explanation
 586 of the observations and as a practical guide for weather forecasting.¹²

587 2.6.2 Basin-scale Rossby waves

588 Satellite altimetry has revealed that most ocean basins are full of low frequency variability. In the lower
 589 subtropics, a portion of the low frequency variability takes the form of very long-crested, westward
 590 propagating, baroclinic features that are unambiguously planetary Rossby waves. These long-crested
 591 waves originate on or near the eastern boundary, and then may propagate a very long distance into the
 592 open ocean (Fig. 14). This phenomenon makes clear that something very close to an elementary Rossby

¹²A classic analysis of westerly waves is available from <http://journals.ametsoc.org/toc/atsc/1/3> An excellent text book reference is http://kiwi.atmos.colostate.edu/group/dave/at605pdf/Chapter_8.pdf A superb animation of westerly waves is at <https://oceanservice.noaa.gov/facts/rossby-wave.html>

593 waves can indeed occur in the ocean, provided that some mechanism has the appropriate (long) time and
 594 (long) space scales needed to generate them in the first place.

595 A remarkable occurrence of such a long-crested Rossby wave was observed in the Pacific ocean in
 596 the decade following the very large amplitude ENSO event of 1982-1983.¹³ The ENSO event began with
 597 a slackening of easterly winds over the western tropical Pacific ocean that allowed the very thick western
 598 tropical thermocline to relax back toward a lower energy state, something like the release of our raised
 599 eddy of Secs. 4.1 and 4.2, though on a much larger scale. The fastest response was a positive (relative
 600 high of SSH and a thick upper layer) Kelvin wave pulse that propagated from the western Pacific to the
 601 eastern boundary of the Pacific (roughly 15,000 km) within about two months; $C \approx 3 \text{ m sec}^{-1}$. The
 602 equatorial Kelvin wave was scattered into positive boundary Kelvin waves that propagated north and
 603 south along the eastern boundary at a similar speed. The arrival of a positive Kelvin wave is accompanied
 604 by warm poleward currents and a thickened thermocline that have very significant consequences for
 605 coastal ecosystems (El Nino of the eastern South Pacific). The thickened thermocline along the eastern
 606 boundary was the proximal forcing mechanism of baroclinic Rossby wave(s) that began propagating
 607 westward across the Pacific basin. The meridional extent of the waves (distance along the wave crest)
 608 was more than 3000 km in both hemispheres, the meridional extent of the boundary Kelvin wave
 609 disturbance. Wave crests were strongly refracted toward the west at low latitudes (Fig. 14), consistent
 610 with the wave speed of long (divergent, non-dispersive) baroclinic Rossby waves, $C \propto \beta/f^2$, i.e., faster
 611 westward propagation at lower latitudes (but not in excess of C). The initial, high SSH wave pulse that
 612 started the 1982-1983 ENSO event was detectable for at least a decade after its generation, by which time
 613 it had reached the western boundary near Japan, where it altered the path of the Kuroshio current. This
 614 kind of very large scale, low frequency variability is predictable for years ahead, once it has formed.

615 One question these observations raise is, how could such a long-crested wave survive the instability
 616 process noted in Sec. 2.7? The satellite SSH observations that were made in the 1980s were not as well
 617 resolved spatially as those made more recently, but a second look at the field of (Fig. 14) suggests that the
 618 wave front may very well have fractured into mesoscale eddies. As we have seen, these eddies propagate
 619 to the west very much like the original, long-crested Rossby wave.

620 2.6.3 Topographic eddies and waves

621 The variation of bottom depth has been omitted from our analysis, mainly for simplicity. This would be
 622 an acceptable approximation in cases where the flow of wind or ocean currents at the ground or sea floor
 623 was very weak, as in the mesoscale eddies of Sec. 2 or the open ocean, equatorial phenomenon of Sec. 3.

¹³Jacobs, G. A., H. E. Hurlburt, J. C. Kindle, E. J. Metzger, J. L. Mitchell, W. J. Teague, and A. J. Wallcraft, 1994: 'Decade-scale trans-Pacific propagation and warming effects of an El Nino anomaly', *Nature*, Vol. 370, pp. 360-363.

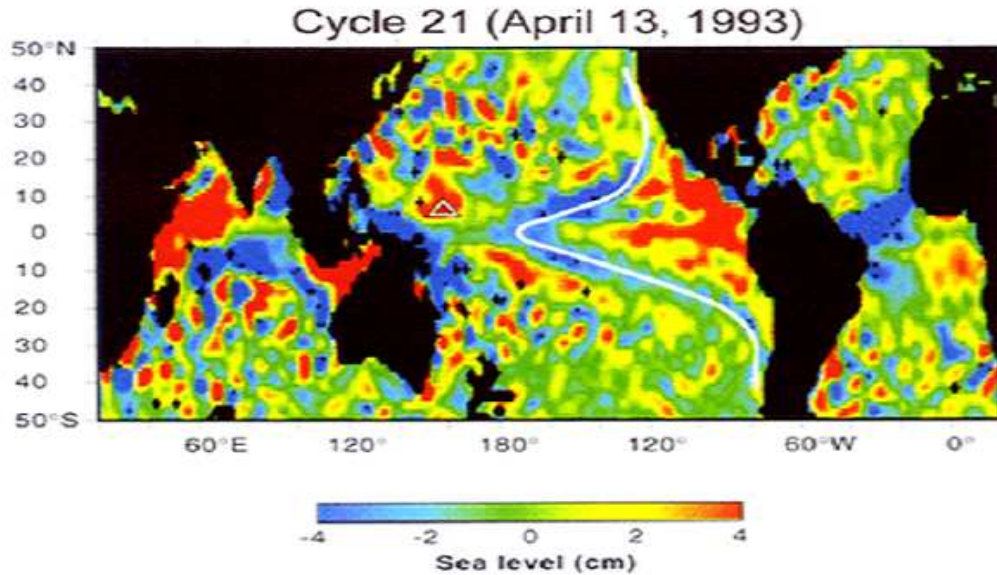


Figure 14: A snapshot of SSH observed by TOPEX/POSEIDON satellite altimetry in the Spring of 1993. The subtropics in both hemispheres of the Pacific basin showed long-crested, westward propagating baroclinic Rossby waves that started on the eastern boundary. The white line is along a relative low of SSH. The westward refraction of the wave crest at low latitudes is consistent with the latitudinal dependence of a long (divergent and non-dispersive) baroclinic Rossby wave. Notice that there is similar variability evident also in the Atlantic basin (though evidently not in 2007, Fig. 2). This figure is reproduced with permission from Dudley Chelton, and is from Chelton and Slax (1994), http://www-po.coas.oregonstate.edu/research/po/research/rossby_waves/chelton.html (may have to be typed in).

624 However, there are common circumstances where strong currents occur near the bottom even in the deep,
 625 stratified ocean, e.g., under the Gulf Stream, and circumstances where the flow is barotropic
 626 (depth-independent) and hence in contact with the bottom, e.g., on continental shelves. The relevant,
 627 background potential vorticity is then $f/(H+b)$, with $H+b(x,y)$ the nominal thickness. The essential
 628 difference between column thickness that varies with b vs. η is that b is spatially dependent but time
 629 independent. A fluid column that moves across bottom contours will then necessarily be stretched (or
 630 squashed), inducing relative vorticity, exactly as does flow across lines of constant f .

631 The ratio of planetary to topographic vorticity change over a typical continental shelf is

$$632 \frac{\text{planetary}}{\text{topographic}} = \frac{\frac{1}{f} \frac{\partial f}{\partial y}}{\frac{1}{h} \frac{\partial h}{\partial y}} = \frac{h}{\alpha R_E} \text{ is } O(10^{-1}),$$

633 given a bottom slope $\alpha = 10^{-3}$ and nominal depth $H = 200$ m. The magnitude of the topographic term
 634 can easily exceed the planetary β term since the bottom depth typically varies on much shorter spatial

635 scales than does f (radius of Earth, R_E). Topographic effects would prevail over the (planetary) β -effect
 636 over most of the deep, open ocean as well, except that stratification largely shields the upper water
 637 column from direct bottom slope effects. Assuming that topographic variation dominates the gradient of
 638 the background potential vorticity, $q = f/H$, and that the flow is depth-independent, then the frequency
 639 of topographic Rossby waves is given by

$$640 \quad \frac{\omega}{f} = \frac{\alpha g}{fC} \left(\frac{R_d K}{1 + R_d^2 K^2} \right),$$

641 where $R_d = C/f$ is the barotropic radius of deformation, with $C = \sqrt{gH}$ computed from a nominal H and
 642 the full gravity. For a nominal shelf, $C \approx 45 \text{ m s}^{-1}$ and $R_d \approx 900 \text{ km}$ (mid latitudes). These waves often
 643 have considerably higher frequencies than do planetary Rossby waves, with 5 - 20 day periods being
 644 common. They have correspondingly greater phase and group speeds as well. Just as planetary Rossby
 645 waves propagate phase westward - with higher background potential vorticity to the right of the wave
 646 vector - so too these topographic Rossby waves propagate phase with shallower water and thus larger
 647 f/H on their right.¹⁴

648 2.6.4 Tropical cyclones

649 One of the most remarkable instances of Rossby wave dynamics occurs in conjunction with tropical
 650 cyclones (TC), intense vortical flows around low pressure anomalies. Most TCs begin with a convective
 651 cloud cluster, that may become organized into a vortex and grow in amplitude and scale if the mesoscale
 652 shear environment includes sufficient cyclonic vorticity. Mature TCs typically have a radius of several
 653 hundred kilometers, which is quite small compared to the atmospheric radius of deformation, about 1000
 654 km.

655 Some tropical cyclones (about 1 in 6) have been observed to develop a marked, eastward-extending
 656 Rossby wave wake in the troposphere. The wavelength along the wake is typically several thousand
 657 kilometers, and consists of alternate cyclonic and anti-cyclonic disturbances. The cyclonic features have
 658 been observed to act as the vorticity trigger for subsequent TC genesis, so that TCs, particularly in the
 659 western North Pacific, may develop in a semi-regular sequence at intervals of several thousand kilometers.
 660 The spatial scale is evidently set by the Rossby wave properties of the eastward extending wake.¹⁵

¹⁴An excellent description of short-crested, baroclinic, topographic waves (or eddies) observed under the Gulf Stream is available at <http://www.po.gso.uri.edu/dynamics/wbc/TRW.html>

¹⁵This phenomenon is an active area of research, see Krouse, K. D. , A.H. Sobel and L. M. Polavni, 2008, 'On the wavelength of the Rossby waves radiated by tropical cyclones', *J. Atmos. Res.*, 65, 644-654, and references therein.

661 **2.7 Problems**

662 (1) Eqn. (13) is the third time that the radius of deformation has arisen as the appropriate length scale
 663 against which to compare (or measure) horizontal scales, in that case the wavelength of Rossby waves.
 664 Does this reflect an excess of enthusiasm for R_d , or is there really nothing else as suitable? What about
 665 the layer thickness, H ? Surely it too is an intrinsic length scale.

666 (2) Rossby waves exhibit normal dispersion in that longer waves have greater phase speed. It can
 667 happen that shorter waves have a greater phase speed, a property dubbed anomalous dispersion. An
 668 example of anomalous dispersion that you can readily investigate is that of capillary waves generated by
 669 the movement of a small object across the surface of still water. If the object moves more slowly than the
 670 slowest gravity/capillary wave, there are no waves. But when the speed of the moving object exceeds this
 671 minimum wave speed, a wave pattern will suddenly appear around and in front of the object. Short
 672 capillary waves lead the pack. Here's a question for you to answer experimentally: at what speed does
 673 this occur? (A factor of two is fine.) Anomalous and normal dispersion may be investigated also via
 674 numerical experiments that solve an initial value problem, ftransform.m (Sec. 7, Part 2).

675 (3) A couple of dispersion relation questions for you: 1) Sketch the dispersion relations for the short and
 676 long Rossby waves limits onto Fig. (6, upper). Use parameters appropriate to 30° N; $f = 7.29 \times 10^{-5}$
 677 sec^{-1} , $C = 3 \text{ m sec}^{-1}$, and $\beta = 1.98 \times 10^{-11} \text{ sec}^{-1} \text{ m}^{-1}$. 2) Discuss the phase and group speed in the case
 678 that $KR_d = 1$, and interpret Fig. (4, lower).

679 (4) Westward energy propagation is the dominant outcome of the β plane experiments and got most of
 680 our attention, but there is noticeable eastward energy propagation as well. Starting with Eqn. (13), show
 681 that the maximum eastward C_g is $C_{longRo}/8$ and occurs at $R_d k_x = \sqrt{3}$.

682 (5) Evaluate the long Rossby wave speed over the latitude range 10° to 50° . In this you may assume that
 683 the gravity wave speed C is constant, $C = 3 \text{ m sec}^{-1}$ (though in fact it decreases somewhat poleward of
 684 the subtropics). You will notice that the latitudinal dependence of the long Rossby wave speed is quite
 685 pronounced. Can you explain in a few words where this f^{-2} dependence originates?

686 (6) Some eddy propagation questions. 1) How does your result from the problem 4) above compare with
 687 the eddy propagation speed found in the numerical experiments? The experiment of Fig. (2) takes care of
 688 30° N, so you will need to find the numerical result for other latitudes. Much better that you design and
 689 run the experiments yourself, but in case that is not feasible, some animations for other latitudes are
 690 linked in Sec. 7, Part 2. We noted in the discussion of Fig. 1 that the observed propagation speed of
 691 oceanic mesoscale eddies varies significantly with latitude, being considerably faster towards lower
 692 latitude. On average over all ocean basins the observed¹ (latitude, zonal speeds) are (10° , $-14 \pm 4 \text{ cm}$
 693 sec^{-1}), (20° , $-5.0 \pm 1.5 \text{ cm sec}^{-1}$), (30° , $-3.5 \pm 1.5 \text{ cm sec}^{-1}$), (40° , $-1.5 \pm 1 \text{ cm sec}^{-1}$) and (50° , $-0.8 \pm$
 694 0.5 cm sec^{-1}). How does this compare with your results above?

695 (7) The natural way to think of conservation is following a given parcel or water column, i.e., a
 696 Lagrangian description. Our model equations are, however, Eulerian. 1) Go back and make an explicitly

697 Lagrangian description of the two q conservation modes discussed above (short and long Rossby waves),
698 and then make the corresponding Eulerian description.

699 (8) The discussion in the main text emphasized the trajectories of the floats that were set inside the
700 initial eddy (the red floats). What happens to the green floats that were launched outside and to the west
701 of the eddy? Consider the small and large amplitude experiments, Figs. (7) and (8) and their animations.

702 3 Adjustment on an equatorial β -plane

703 The temporal and spatial variability of equatorial SSH is very different from that seen at subtropical and
704 higher latitudes. Mesoscale eddies are uncommon (though appear seasonally in some years in the
705 Pacific), and a gyre-like structure is not readily apparent.¹⁶ The main features are:

706 **1) The primary variability of SSH is in zonally elongated features.** These have a meridional scale of
707 several hundreds of kilometers, and widths that may span most of the Atlantic basin. These features
708 exhibit strong seasonality.

709 **2) SSH variability has small amplitude.** Aside from the western boundary current, the amplitude of
710 SSH variability is typically ± 0.05 m, compared with ± 0.1 to 0.2 m for mesoscale eddies of the
711 subtropics and ± 1 m over the subtropical and subpolar gyres. f is, of course, much smaller, and so this
712 does not mean that currents are also small amplitude.

713 **3) Episodic, eastward propagation over distances that may span most of the basin.**¹⁶ The
714 propagation speed of these eastward-going events is comparable to the gravity wave speed, several
715 hundred km per day.

716 3.1 An equatorial adjustment experiment

717 The plan for this section is to carry out a geostrophic adjustment experiment on an equatorial beta-plane
718 ocean and compare the results to previous experiments. As before, the motive is to gain some insight into
719 the properties and mechanisms of the observed SSH noted above. To be sure, the results of this
720 adjustment experiment can account for only a part of these equatorial phenomena, much of which is due

¹⁶Most of the equatorial phenomena described here are seen much better in multi-year records: a superb animation of 18 years of satellite-derived altimetric data including the Pacific and Indian oceans is available from <http://podaac.jpl.nasa.gov/node/430>

721 instead to forcing by the large-scale, time-dependent equatorial winds. Hence, some of the discussion is
 722 deferred to Part 4. Here in Part 3 we will emphasize the properties of equatorial waves, which are of first
 723 importance in understanding variability generally.¹⁷

724 The β -plane is set to $f_0 = 0$ and $f = \beta y$, i.e., an equatorial β -plane. The stratification was changed
 725 somewhat to reflect the shallower main thermocline of equatorial regions, $H = 250$ m, and larger density
 726 contrast across the main thermocline, $\delta\rho = 3 \text{ kg m}^{-3}$. The gravity wave speed $C = \sqrt{g'H} \approx 2.5 \text{ m sec}^{-1}$.
 727 The initial condition is a raised, cylindrical thickness anomaly with radius $L = 200$ km that is centered on
 728 the equator. Though this eddy is twice the size used previously, it is nevertheless small compared to the
 729 intrinsic horizontal scale of the equatorial ocean. The domain is a box 5000 km by 5000 km. The
 730 northern and southern sides are treated with a radiation boundary condition that allows the passage of
 731 gravity waves off of the model domain. The eastern and western sides are defined by zero normal flow,
 732 $u(x = \pm 2500) = 0$. Waves reaching the zonal boundaries are thus reflected and scattered.

733 Soon after the equatorial thickness anomaly is released, Fig. (15), gravity waves propagate away in
 734 all directions. The leading edge of the expanding wave front is nearly circular, and grows in radius at the
 735 gravity wave speed $C = \sqrt{g'H}$, as seen before. Within about a week, gravity wave motions dispersed
 736 (spread) the eddy energy over most of the model domain. The initial thickness anomaly collapsed within
 737 about $L/C \leq 1$ day, very much as would be expected in the complete absence of rotation (Sec. 3.1, Part
 738 2). The initial condition was symmetric about the equator, and this north-south symmetry is maintained
 739 in all that follows. However, the waves showed some significant east-west anisotropy, with preferred
 740 propagation along the equator and especially eastward, as will be discussed further below. These very
 741 significant details aside, this equatorial adjustment process looks more like the pure gravity wave
 742 experiment of Sec. 3 Part 2 than the mid-latitude f - or β -plane experiments. Beta is almost the same in
 743 this experiment as in the mid-latitude experiments of Sec. 2, and so it isn't β alone that matters but
 744 mainly f_o (which is zero here).

745 3.2 An equatorial radius of deformation

746 In the f -plane and mid-latitude β -plane experiments of previous sections, the radius of deformation,
 747 $R_d = C/f_0$, was the intrinsic horizontal scale against which to measure the radius of the initial eddy,
 748 wavelengths, etc. On an equatorial β -plane, $f_0 = 0$, and so the equivalent radius of deformation, R_{deg} , is
 749 bound to be somewhat different. How might this R_{deg} be deduced? Three possibilities: 1) Look for the

¹⁷The GFD text by Gill noted in footnote 1 of Part 2 has a very useful discussion on equatorial dynamics. One of the seminal research papers on equatorial dynamics is also highly recommended: Matsuno, T., 1966, 'Quasi-geostrophic motions in an equatorial area', *J. Met. Soc. Japan*, 44(1), 25-43.

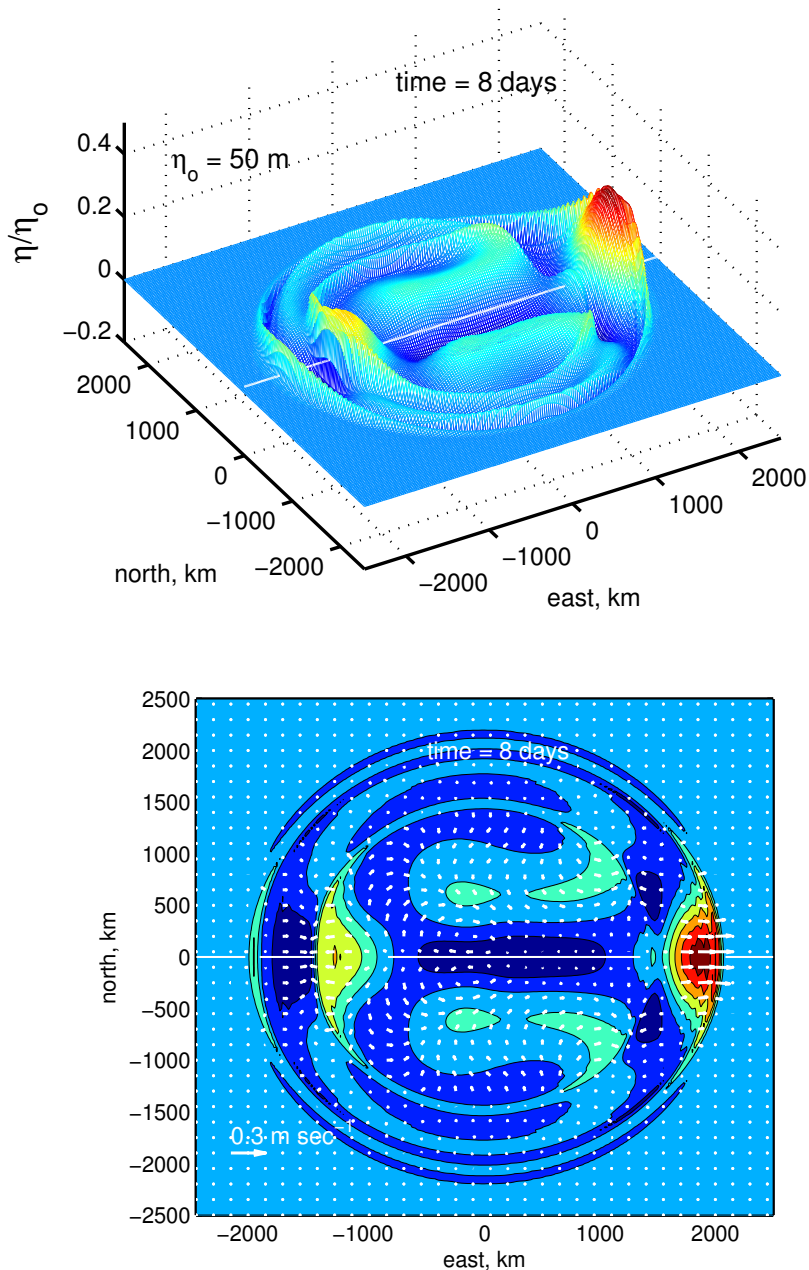


Figure 15: A snapshot from an equatorial adjustment experiment at time = 8 days after releasing a raised eddy centered on $(east, north) = (x, y) = (0, 0)$. The model domain extended 2500 km north and south of the equator (the thin white line), and sidewalls were placed at $x = \pm 2500$ km. East is to the right. (The Pacific Ocean has more than three times this width.) **(upper)** The thickness anomaly, η . Notice that the largest feature is a positive bump centered on the equator and propagating eastward, evidently a Kelvin wave pulse as discussed in the main text. An animation of these data is www.whoi.edu/jpweb/eqtr-eta.flv **(lower)** A plan view of the velocity, and color contours of η . Notice that velocity is generally normal to the η contours, indicating that these fields are mostly gravity wave motion. An animation of this data is www.whoi.edu/jpweb/eqtr-velocity.flv.

750 radius of deformation in a solution involving transcendental functions of the north-south coordinate. An
 751 example is coming in the next section, but very often an explicit solution will not be available, and then
 752 something more general will be required. 2) Apply the method of dimensional analysis to deduce a
 753 length scale from the parameters that define the ocean model. Dimensional analysis works particularly
 754 well in this instance because there are only two parameters that define a shallow water, equatorial
 755 β -plane, the gravity wave speed, C [length time⁻¹] and of course β [length⁻¹ time⁻¹]. The simplest,
 756 dimensionally consistent form of a length is

$$757 \quad R_{deq} = \sqrt{C/\beta}, \quad (28)$$

758 which turns out to be correct. This result came awfully easily, but without the slightest hint of a physical
 759 interpretation. 3) Finally, recall that the long Rossby wave speed increases toward lower latitude as
 760 $\beta R_d^2 = \beta C^2 / f^2$ and on an equatorial beta-plane, $\beta C^2 / (\beta y)^2$. This cannot hold all the way to the
 761 equator, $y = 0$, since the fastest possible wave in the shallow water model is the gravity wave speed, C . At
 762 what y does the long Rossby wave speed equal the gravity wave speed? Again the answer is $y = \sqrt{C/\beta}$,
 763 and now with a very slim hint at an interpretation.

764 Given the (baroclinic) gravity wave speed, $C \approx 2.5 \text{ m sec}^{-1}$, $R_{deq} = 340 \text{ km}$. The local inertial
 765 period at that y is $2\pi/f = 4 \text{ days}$. From this it appears that the eddy defined in the initial condition, radius
 766 $L = 200 \text{ km}$, is small insofar as $L/R_{deq} \approx 1/2$ and it has been noted that the initial eddy was entirely
 767 dispersed into waves. The same result obtains even for a much larger eddy, $L = 500 \text{ k}$, see
 768 www.whoi.edu/jpweb/eqtr_largeeddy.mp4

769 3.3 Dispersion relation of equatorially-trapped waves

770 Wave properties of the equatorial β -plane are clearly very important, and it wouldn't be exaggerating to
 771 say that waves of one kind or another are all that there is this adjustment experiment. For the purpose of
 772 examining wave properties it will be necessary to work with the linear shallow water system; substituting
 773 $f = \beta y$,

$$774 \quad \frac{\partial h}{\partial t} = H \left(\frac{\partial u}{\partial x} + \frac{\partial v}{\partial y} \right), \quad (29)$$

$$775 \quad \frac{\partial u}{\partial t} = -g' \frac{\partial h}{\partial x} + \beta y v, \quad (30)$$

$$776 \quad \frac{\partial v}{\partial t} = -g' \frac{\partial h}{\partial y} - \beta y u. \quad (31)$$

779 Presuming the existence of zonally propagating waves that have an unknown y -dependence, then for the
 780 meridional velocity (this follows very closely the classic paper by Matsuno¹⁷);

$$781 \quad v(x, y, t) = V(y) \cos(kx_x - \omega t), \quad (32)$$

782 and similarly for $U(y)$ and $\Upsilon(y)$. By substitution into the linear shallow water equations and after
 783 eliminating $U(y)$ and $\Upsilon(y)$ by cross-differentiating and adding (as in the derivation of the potential
 784 vorticity balance) there results a second order, ordinary differential equation for $V(y)$,

$$785 \quad \frac{d^2V}{dy^2} - \left(\frac{\beta^2 y^2}{C^2} - \frac{\omega^2}{C^2} + \frac{\beta k_x}{\omega} + k^2 \right) V = 0, \quad (33)$$

786 and a dispersion relation discussed below. To be physically realizable,

$$787 \quad V(y) \rightarrow 0 \text{ as } |y| \rightarrow \infty. \quad (34)$$

788 Eqns. (33) and (34) have the form of a Shrodinger equation for a quantum harmonic oscillator, and the
 789 solutions are the set of eigenfunctions

$$790 \quad V_n(y) = \exp\left(-\frac{y^2}{2R_{deq}^2}\right) H_n\left(\frac{y}{R_{deq}}\right)$$

791 where H_n is the n th (physicist's) Hermite polynomial. The first five are $H_0 = 1$, $H_1 = 2y$, $H_2 = 4y^2 - 2$,
 792 and $H_3 = 8y^3 - 12y$. The eigenfunctions $V_n(y)$ are meridional normal modes that are numbered $n = 0, 1, 2$
 793 etc. (Fig. 16, right). The Kelvin mode labeled $n = -1$ requires a separate discussion to follow. The
 794 eigenfunctions of the interface displacement, $\Upsilon_n(y)$, may be computed from the $V_n(y)$ as,¹⁷

$$795 \quad \Upsilon_n(y) = 0.5(\omega R_{deq}/C - k_x R_{deq})V_{n+1}(y) - n(\omega R_{deq}/C + k_x R_{deq})V_{n-1}(y). \quad (35)$$

796 The odd numbered $\Upsilon_n(y)$ are symmetric about the equator, i.e., $\Upsilon_n(y) = \Upsilon_n(-y)$ (Fig. 16, right), while the
 797 even-numbered modes are anti-symmetric, $\Upsilon_n(y) = -\Upsilon_n(-y)$. This symmetry is very consequential for
 798 the excitation of the normal modes.

799 The dispersion relation $\omega(k)$ is

$$800 \quad \omega^3 - \left(C^2 k_x^2 + \frac{(2n+1)C^2}{R_{deq}^2} \right) \omega - \beta C^2 k_x = 0, \quad (36)$$

801 where k is the zonal wavenumber (there is no north-south wavenumber by virtue of Eqn. 32), and n is the
 802 (meridional) mode number. This dispersion relation is cubic and so looks a bit complicated. However, its
 803 graph, Fig. (16, left) reveals two familiar wave types — higher frequency waves that are close analogs of
 804 the mid-latitude inertia-gravity waves, and lower frequency Rossby waves. As in the mid-latitude
 805 β -plane experiment, there is a significant frequency gap between the lowest frequency inertia-gravity
 806 wave, $\omega R_{deq}/C \approx 1.7$ (dimensional period = 5.4 days), and the highest frequency Rossby wave,
 807 $\omega R_{deq}/C \approx 0.3$ (period = 30 days).

808 The equatorial β -plane also supports two important wave types that are not found in the

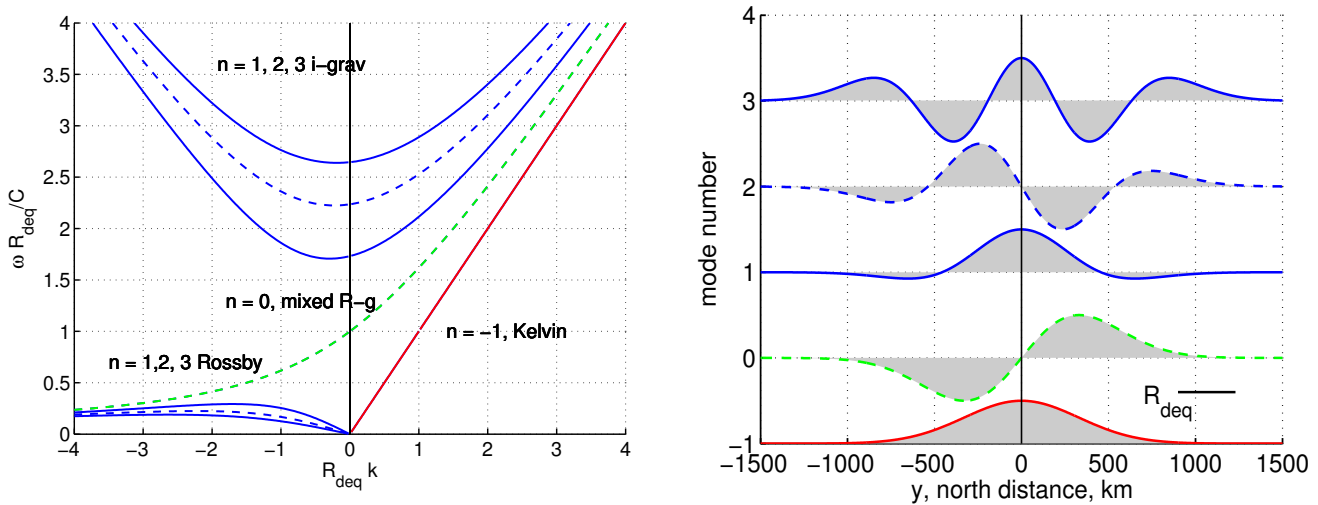


Figure 16: **(left)** Dispersion diagram for the trapped waves on an equatorial β -plane. The modes are numbered $n = -1, 0, 1, \dots$ etc. The Kelvin wave $n = -1$ is in red, the mixed Rossby-gravity wave is in green dashed, and the inertia-gravity and Rossby waves are in blue. Modes that are symmetric in $\eta(y)$ are solid, while modes that are anti-symmetric are dashed. Note that the equatorial radius of deformation is used to nondimensionalize the zonal wavenumber, k_x , and the equatorial inertial period R_{deq}/C used to nondimensionalize the frequency. **(right)** The meridional modes of η , $Y_n(y)$, computed from the $V(y)$ modes and Eqn. (35) using $\omega R_{deq}/C \approx 2$ and $R_{deq}k_x \approx -1$, appropriate to westward propagating inertia-gravity waves. For Rossby wave values, the details are different, but the symmetry properties of the modes remain the same. The colors correspond to those at left, e.g., the Kelvin wave is in red. The amplitudes are arbitrary. Notice that lower numbered modes are effectively trapped near the equator, while higher modes may have an appreciable amplitude at higher latitudes.

809 mid-latitude, open ocean. 1) The mode $n = 0$, appropriately called a mixed Rossby-gravity wave, has a
 810 $\omega(k)$ that closely parallels the Rossby wave modes for negative wave numbers (west-going waves), and
 811 parallels the inertia-gravity waves for positive wave numbers (east-going waves). The group speed of
 812 these waves is eastward at all frequencies. Depending upon the wavenumber, Rossby-gravity waves can
 813 have a frequency that is intermediate between the low frequency Rossby waves and the higher frequency
 814 inertia-gravity waves. Hence, there is no frequency gap in the family of free equatorial waves, as occurs
 815 at mid-latitudes. Unfortunately, these waves are not observed in the present experiment, because the
 816 mixed Rossby-gravity wave mode is anti-symmetric in $\eta(y)$ and so is not excited by the symmetric,
 817 initial thickness anomaly used here. 2) Second, the equatorial beta-plane also supports an eastward-going
 818 Kelvin wave, of which more below.

819 **3.3.1 Westward-going gravity and Rossby waves**

820 The most noteworthy wave motions appear to be trapped near the equator (Figs. 15 and 16). First,
 821 consider the wave motion(s) that are farthest west of the origin, $-2000 < x < -1800$ km, at time = 8
 822 days. The velocity is almost normal to isolines of η and thus longitudinal and gravity wave-like. The
 823 meridional structure is a single maximum of meridional extent approx. R_{deq} , that is symmetric about the
 824 equator and thus meridional mode $n = 1$. The dominant wavelength is very roughly $\lambda = 1000$ km so that
 825 $kR_{deq} \approx 2$. In this $R_{deq}k_x$ range, the dispersion relationship for gravity waves is dispersive, and the group
 826 speed is slightly less than the maximum possible, $\sqrt{g'H}$. The $\eta(x)$ profile looks wave-like, vs. pulse-like
 827 (Figs. 17 and 18) Thus the leading, west-going waves appear to be equatorially-trapped gravity waves.

828 A somewhat larger amplitude westward-going feature trails behind the leading gravity waves; at
 829 time = 8 days a local maximum is centered on $(x, y) = (-1200, 0)$ km. The meridional structure is very
 830 similar to that noted above, mode $n = 1$, and Gaussian with north-south scale R_{deq} . The group speed is
 831 evidently about half or less of the fastest westward-going gravity waves noted just above. A qualitative
 832 difference with the gravity waves is that the velocity has some component along isolines of thickness,
 833 rather than normal as for gravity waves, and hence the velocity is somewhat geostrophic. These
 834 properties are consistent with a meridional mode 1 equatorial Rossby wave. Equatorial Rossby waves
 835 have a dispersion relation that is the low frequency limit of Eqn. (36),

$$836 \quad \omega = -\frac{Ck_x}{R_{deq}^2 k_x^2 + (2n+1)}. \quad (37)$$

837 The long wave limit, $R_{deq}^2 k_x^2 \ll 1$, for $n = 1$ has phase and group speed

$$838 \quad C_p = C_g = \frac{C\omega}{k_x} = -C/3$$

839 or about 100 km per day and westward. These long Rossby waves are nondispersive (although for the
 840 west-going waves considered as a whole there is clearly a significant range of phase and group speeds). It
 841 is notable that long equatorial Rossby waves have phase and group speed that are greater by a factor of
 842 about 30 than that of mid-latitude, long Rossby waves. This has great significance for the response of the
 843 equatorial ocean to seasonally varying wind stress, as we will discuss in Part 4.

844 **3.3.2 Kelvin wave**

845 The eastward-going motion is made up mainly of a very prominent isolated maxima in η that has the
 846 propagation properties of an equatorial Kelvin wave. This Kelvin wave pulse is important and interesting

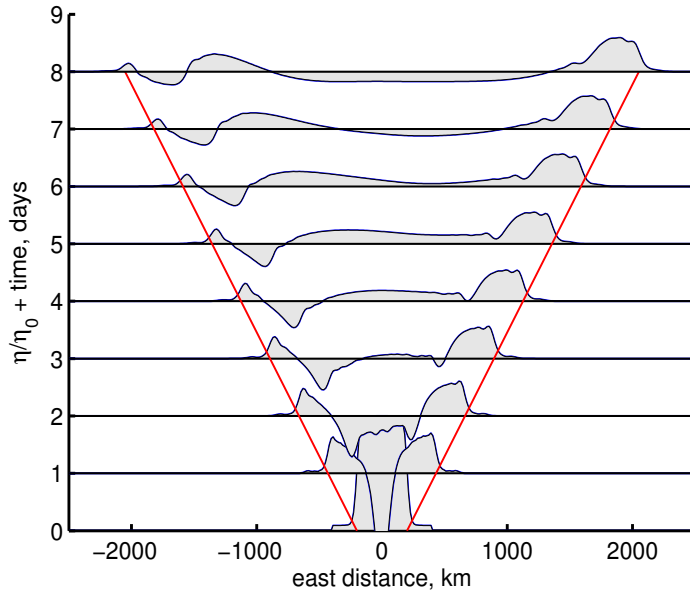


Figure 17: A series of slices through the numerical solution Fig. (15) along the equator showing $\eta(x, y = 0, \text{time} = 0, 1, 2, \dots \text{ days})$ normalized by $\frac{1}{2}\eta_0$. The red lines have a slope $= dx/dt = \pm C = \pm\sqrt{g'H}$. Notice that the westward-going, gravity wave packet changes shape with time and has only a small mean value. The eastward-going Kelvin wave pulse maintains a nearly constant shape and has an appreciable mean value. This illustrates the often qualitative difference between dispersive (westward-going) and nondispersive (eastward-going) wave propagation.

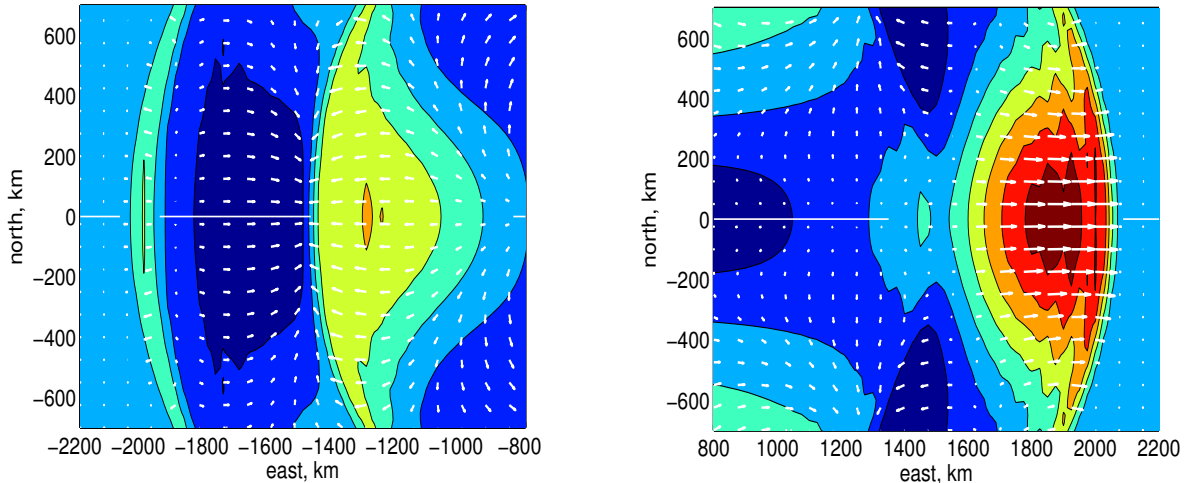


Figure 18: Enlarged snapshot views at time = 8 days of the equatorially-trapped, westward- and eastward-going local maxima from Fig. (15). **(left)** The westward-going pulse is dispersed into faster-moving gravity waves and slower moving, somewhat larger amplitude Rossby wave(s). Both kinds of westward propagating waves are evidently meridional mode 1 (Gaussian). **(right)** The eastward-going wave pulse has the properties of a Kelvin wave; the north-south structure is Gaussian, as at left, and the fluid velocity (the field of small white arrows) is directed almost exclusively east-west and

847 on two counts: first, it is the biggest feature in the solution, and second, it does not appear as a solution of
848 the modal equation (33).

849 Suppose we did not know that this feature was a Kelvin wave — could we infer the dynamics from
850 the properties evident in the numerical solution? Several useful clues are evident in a sequence of
851 equatorial slices through the solution, Fig. (17), and in a magnified plan view, Fig. (18).

- 852 1. The pressure/velocity relationship is mainly longitudinal and the velocity is almost entirely zonal
853 (east-west). Hence there is little or no β effect. These characteristics are consistent with a gravity
854 wave, but not a Rossby wave.
- 855 2. Once this feature is separated from the initial eddy, the zonal wave form $\eta(x)$ remains almost
856 constant as it propagates eastward at a speed very close to the gravity wave speed, $C = \sqrt{g'H}$. This
857 is evidence of a nondispersive gravity wave motion as in Part 2, Sec. 3.1.
- 858 3. The meridional profile $\eta(y)$ is symmetric across the equator and is nearly self-similar, suggesting
859 an equatorially-trapped wave mode. The half-width in y is about 400 km, or roughly R_{deq} .

860 The most telling/important clue to the dynamics is perhaps the first one, that $v = 0$. When this is
861 implemented in the linear shallow water equations the result is a significantly reduced set:

$$862 \quad \frac{\partial \eta}{\partial t} = H \frac{\partial u}{\partial x}, \quad (38)$$

$$863 \quad \frac{\partial u}{\partial t} = -g' \frac{\partial \eta}{\partial x}, \quad (39)$$

$$864 \quad 0 = -g' \frac{\partial \eta}{\partial y} - \beta y u. \quad (40)$$

867 Eqns. (38) and (39) are exactly the pure gravity wave (nonrotating) system of Sec. 3.1 Part 2 and
868 lead to the same elementary wave equation in (x, t) ;

$$869 \quad \frac{\partial^2 \eta(x, y, t)}{\partial t^2} = g'H \frac{\partial^2 \eta(x, y, t)}{\partial x^2}, \quad (41)$$

870 and the familiar phase speed,

$$871 \quad \frac{\omega}{k} = \sqrt{g'H} = C.$$

872 This phase speed does not depend upon k_x , and so this wave is nondispersive, which is consistent with the

873 observed wave form Fig. (18). Eqn. (40) indicates a geostrophic balance for the east-west component of
 874 the velocity. Substitution of the updated Eqn. (32) into Eqn. (40) gives

$$875 \quad 0 = \frac{d\Upsilon(y)}{dy} - \frac{\beta\omega}{g'Hk_x}y\Upsilon(y). \quad (42)$$

876 Together with the boundedness requirement, this yields the y -dependence of the pulse shape, a Gaussian
 877 $\propto \exp(-y^2/2R_{deq}^2)$, where $R_{deq} = \sqrt{C/\beta}$. Combining these two results gives a partial solution

$$878 \quad \eta(x, y, t) = \eta_0(x) \exp\left(\frac{-y^2}{2R_{deq}^2}\right) \cos(k_x x - \omega t), \quad (43)$$

879 where $\eta_0(x)$ is the zonal width of the Kelvin wave pulse. The important qualitative results from this brief
 880 analysis are: 1) an equatorial Kelvin wave propagates eastward only, 2) it is non-dispersive, 3) it is
 881 symmetric across the equator (Fig. 16, right) and 4) it has a Gaussian zonal profile and zonal scale R_{deq} .
 882 The meridional profile is always the Gaussian of (43), regardless of the initial eddy size. However the
 883 width of the wave pulse, $\eta_0(x)$, is proportional to the width of the initial eddy, rather short in this
 884 experiment.

885 Because an equatorial Kelvin wave has zero meridional fluid velocity, it is not represented in the
 886 second order equation (33) for the meridional structure $V(y)$. Thus Eqn. (33) contains only a subset of the
 887 shallow water system, that having meridional velocity. The Kelvin wave has to be added to the solutions
 888 of Eqn. (33) in order to make a complete set and, more to the point, to account for the phenomenon seen
 889 in our numerical experiment. The Kelvin wave is usually assigned the label $n = -1$, since it's dispersion
 890 properties $\omega(k)$ fit Eqn. (36) for that n . Since there is no meridional flow across the equator, the equator
 891 could just as well be replaced by a (frictionless) wall insofar as the Kelvin wave alone is concerned.

892 The Kelvin wave is clearly a very important part of the adjustment process: inertia-gravity and
 893 Rossby waves carry energy away from the collapsing eddy, but the Kelvin wave pulse carries energy
 894 along with roughly 2/3 of the excess layer thickness (initial eddy volume) towards the east. When the
 895 Kelvin wave pulse reaches the eastern boundary it is partially reflected back to the west in the form of
 896 equatorially-trapped inertia-gravity and Rossby waves. Most of the volume contained within the
 897 equatorial Kelvin wave is scattered onto boundary-trapped Kelvin waves that propagate north and south
 898 along the eastern boundary of the model domain (to see this you will need to view the animation linked in
 899 the caption to Fig. 15).¹⁸

¹⁸An excellent online reference for the role of equatorial waves in the ENSO phenomenon is available
 at <http://iri.columbia.edu/climate/ENSO/theory/index.html> More on the equatorial Kelvin wave may be found at
http://science.nasa.gov/science-news/science-at-nasa/2002/05mar_kelvinwave/ (may have to be typed into your web browser).

900 3.4 Problems

901 (1) Some Kelvin wave questions for you. 1) In our geostrophic adjustment experiment the initial eddy
 902 had a positive η (easier to plot); suppose instead the initial eddy was a depression in the layer thickness;
 903 what differences might be expected for the Kelvin wave? Consider also finite amplitude effects that you
 904 can check with the numerical model. 2) Is it possible to have an equatorial Kelvin wave that propagates
 905 westward? 3) The zonal velocity of a Kelvin wave is in geostrophic balance with the tilted interface. Can
 906 you show that the resulting $u(y)$ is also consistent with one of the potential vorticity conservation modes
 907 discussed in Sec. 2.2.3, Part 2? 4) How would the Kelvin wave change if the initial eddy was made larger
 908 or smaller in the horizontal?

909 (2) The north-south symmetry of the initial condition chosen here had significant consequences for the
 910 waves that were generated during geostrophic adjustment. Suppose that the initial eddy was displaced off
 911 of the equator - what might be different? This is something you can check with a numerical experiment.

912 4 Summary and Remarks

913 This essay started with the question **What processes lead to the marked east-west asymmetry that is**
 914 **observed to characterize most large scale circulation (low frequency) phenomena?** Important
 915 examples of this asymmetry evident in Fig. (1) include the westward propagation of mesoscale eddies
 916 and the very marked westward intensification of the wind-driven gyres. This essay has emphasized the
 917 β -effect that arises from the northward variation of f combined with meridional velocity.

918 4.1 Mid-latitude mesoscale eddies

919 The first experiments considered in Sec. 2 included the geostrophic adjustment of a mesoscale-size
 920 thickness anomaly released onto a mid-latitude β -plane.

921 **1) The short-term (several days) geostrophic adjustment process is little altered by β .** The
 922 inertia-gravity waves that propagate poleward are, however, reflected when they reach a latitude where f
 923 is comparable to their intrinsic (initial) frequency. This β -induced reflection is an interesting and
 924 important process for inertia-gravity waves found in the open ocean, but it has no evident effect upon the
 925 adjusted eddy.

926 **2) The long-term (weeks to months) evolution of a nearly balanced eddy includes β -induced**
 927 **westward propagation** that is absent on an f -plane. For typical, subtropical C and f (30° N) the eddy

928 peak moves westward at about 3 km day^{-1} . The propagation speed increases sharply toward lower
 929 latitude. The numerical eddies studied here appear to make a good analog of oceanic mesoscale eddies
 930 (Fig. 1) insofar as they reproduce approximately the latitudinally-dependent zonal propagation of the
 931 eddies observed in SSH (problem 2.9.8). The β -effect acting upon nearly geostrophic eddies is a highly
 932 plausible mechanism for the observed, westward propagation of oceanic mesoscale eddies.

933 **3) The β -plane shallow water system supports a low frequency wave, a planetary Rossby wave,
 934 that make a very useful analog of mesoscale eddies.** Outside of the tropics, baroclinic, planetary
 935 Rossby waves have a low frequency, typically only about one percent of f , and currents that are nearly
 936 geostrophic. Rossby waves are markedly anisotropic in that they propagate phase westward only.
 937 Elementary (plane) Rossby waves are not commonly observed in the ocean or atmosphere but they are of
 938 great interest here because they have time and space scales in common with mesoscale eddies, and long
 939 baroclinic Rossby waves exhibit a very similar potential vorticity balance, β balanced by stretching. The
 940 phase and group speed of long, nondispersive Rossby waves is $-\beta/R_q^2$ (westward), which is just slightly
 941 greater than the propagation speed of the numerical mesoscale eddies, including the marked latitudinal
 942 dependence.

943 **4) Insofar as westward propagation alone is concerned, the numerical eddies look to be an
 944 essentially linear phenomenon.** However, their amplitude measured by thickness anomaly is
 945 appreciable, $\delta h/H \approx 0.1$, and their typical currents are several times greater than their propagation speed.
 946 As a consequence, they are likely able to trap and transport tracer for an appreciable distance. Insofar as
 947 transport goes, the numerical eddies exhibit important finite amplitude effects.

948 4.2 Equatorial Adjustment

949 **5) The equatorial region — aside from the western boundary — appears to be almost free of
 950 mesoscale eddy variability ($L \propto$ several hundred km).**¹⁹ An adjustment experiment set up in an
 951 equatorial ocean suggests one reason for this may be that anomalies with horizontal scales $L < 500 \text{ km}$
 952 will disperse into gravity and Rossby waves before adjusting to geostrophy. This is an extension of the
 953 main result from Sec. 4 Part 2 that the fraction of an initial anomaly that survives geostrophic adjustment
 954 is dependent upon the ratio L/R_{deq} , where the equatorial radius of deformation is $R_{deq} = \sqrt{C/\beta} = 250$
 955 km and about five times greater than the mid-latitude equivalent.

956 **6) Eastward propagation of a Kelvin wave is the most prominent feature of the equatorial**

¹⁹Mesoscale eddy-like features do appear seasonally some years, in especially the North Pacific equatorial ocean. These eddies are thought to result from an instability of the wind-driven equatorial current system and are termed Tropical Instability Waves. An excellent, brief introduction is http://en.wikipedia.org/wiki/Tropical_instability_waves

957 **adjustment experiments studies here** (in part due to the symmetric initial condition) and is an
 958 occasional and sometimes very prominent feature also of the real equatorial oceans. The Kelvin wave has
 959 phase and group speed equal to the gravity wave speed, and is nondispersive. A Kelvin wave that is
 960 generated in mid-ocean (say by a rapid change in the winds) will thus reach the eastern boundary in a
 961 matter of weeks. There it is scattered into boundary Kelvin waves that propagate north and south along
 962 the eastern boundary of both hemispheres, and to a lesser extent, into westward traveling, dispersive,
 963 equatorially-trapped gravity and Rossby waves.

964 **7) The equatorial ocean differs from the midlatitude beta-plane ocean in that the frequency gap**
 965 **between inertia-gravity waves and Rossby waves is much smaller;** the inertia-gravity waves have a
 966 comparatively low (dimensional) frequency, and the Rossby waves a comparatively high frequency and
 967 fast group speed. As we will see in Part 4, this has the consequence that the equatorial ocean adjust
 968 comparatively very rapidly to changing wind stress, including annual variations.

969 4.3 Remarks

970 An important result implicit in 1) above is that a mid-latitude β -plane supports two distinctly different,
 971 and for the most part non-interacting kinds of waves and associated dynamics: fast time-scale
 972 inertia-gravity waves and slow time-scale, quasi-geostrophic Rossby waves and eddies. This has practical
 973 importance on several levels. Insofar as westward propagation goes, it would have been simpler to start
 974 the experiment with a balanced eddy and forego the geostrophic adjustment and inertia-gravity waves.
 975 There is a pedagogic aspect as well. It is sensible to introduce geostrophic adjustment and Rossby wave
 976 dynamics as separate topics, rather than conflated as they have been here. The rationale for considering
 977 these phenomenon in the same experiment is partly that the clear separation of time scales and dynamics
 978 that characterizes mid-latitudes does not extend to the equatorial region where inertia-gravity waves and
 979 Rossby waves have overlapping time and space scales, 6).

980 The present numerical experiments start from a highly idealized initial condition, a right cylinder of
 981 thickness anomaly having a specified radius and that is released into a still ocean. The sudden release of
 982 this anomaly produces a fairly broad wavenumber and frequency spectrum, including gravity waves and
 983 short Rossby waves having eastward (but very small) group speed. This is not realistic of actual oceanic
 984 mesoscale eddies that are formed from a comparatively slowly growing instability of larger-scale, nearly
 985 geostrophic currents, e.g., a Rossby wave Sec. 2.7, and so are close to geostrophic balance from the
 986 outset. A fairly crude representation of this follows from initializing an adjustment experiment with a
 987 very large eddy, say radius $L = 1000$ km, or more to the point, $L = 20R_d$. The central portion of this eddy
 988 remains flat and at rest after the edges have adjusted to geostrophy. The subsequent evolution of this eddy
 989 is quite different from the propagation of a long Rossby wave, and neither is it anything like a small,

990 wind-driven gyre. The southerly flow along the western edge is unstable and spontaneously forms eddies
991 having a diameter of about 300 km. These eddies are very similar to the eddies made here by geostrophic
992 adjustment from a state of rest, although a little larger. This eddy formation process likely has some
993 important elements in common with the formation of real oceanic mesoscale eddies, though lacking
994 adequate vertical resolution.

995 In regions having intense currents, e.g., the Gulf Stream and extension of Fig. 1, the ocean is
996 teeming with mesoscale eddies, not eddies in isolation in a homogeneous environment as presumed here.
997 There are other kinds of oceanic variability and of course, sea floor topography. Interactions between
998 neighboring eddies and between eddies and the atmosphere give rise to phenomena that modify the
999 eddies and the larger scale environment significantly.²⁰

1000 4.4 What's next?

1001 Part 4 will study basin scale, wind-driven flow using the same shallow water model but augmented with a
1002 body force that mimics wind stress. The aim will be to elucidate the mechanism(s) that lead to western
1003 intensification of the major ocean gyres. It will also become clear that eddies and gyres are in some ways
1004 close cousins since they have a similar beta effect which is balanced by time dependence, or by wind
1005 stress curl and divergent Ekman transport.

²⁰McGillicuddy, D., et al., 'Eddy/wind interactions stimulate extraordinary mid-ocean plankton blooms', *Science*, 316, 1021 (2007), DOI: 10.1126/science.1136256 See also Chelton, D. B., P. Gaube, M. G. Schlax, J. J. Early and R. M. Samelson, 'The influence of nonlinear mesoscale eddies on near-surface oceanic chlorophyll', *Science*, 334, 21 Oct 2011, 328-332, doi: 10.1126/science.1208897

Index

- 1006 anisotropic, 13
- 1007 beta, 5
- 1008 beta effects, 5
- 1009 beta-plane
- 1010 equatorial, 36

- 1011 eddies and waves, 14
- 1012 eddy propagation
- 1013 meridional, 21
- 1014 eddy properties, 6
- 1015 eddy westward propagation, 7
- 1016 equatorial waves
- 1017 dispersion relation, 40

- 1018 floats, 26

- 1019 inertia-gravity waves, 9

- 1020 Kelvin wave, 43

- 1021 passive tracer, 24
- 1022 potential vorticity balance, 11
- 1023 propagation
- 1024 finite amplitude effects upon, 21

- 1025 radiation boundary condition, 10
- 1026 radius of deformation
- 1027 equatorial, 37
- 1028 Rossby wave
- 1029 short wave limit, 17
- 1030 basin scale, 31
- 1031 dispersion relation, 15
- 1032 equatorial, 42
- 1033 instability, 28
- 1034 long wave limit, 19
- 1035 topographic, 32
- 1036 westward phase speed, 15

- 1037 Rossby waves, 14
- 1038 westerly waves, 30